Enzymatic Activity and Excited State Processes in Protochlorophyllide Oxidoreductase

Sytina, O.

2010

~ CHAPTER 3 ~

Enzymatic photoconversion of Protochlorophyllide in NADPH:protochlorophyllide oxidoreductase characterized by ultrafast visible pump-probe spectroscopy and kinetic modeling

Olga A. Sytina, Ivo H.M. van Stokkum, Derren J. Heyes, C. Neil Hunter, Rienk van Grondelle and Marie Louise Groot

The enzyme NADPH:protochlorophyllide oxidoreductase (POR) catalyses the reduction of protochlorophyllide into chlorophyllide, a precursor of chlorophyll a in photosynthetic organisms. Here, we present ultrafast spectroscopic experiments carried out under single pulse conditions, which confirm that initially inactive enzyme complexes become active upon absorption of a first photon, and a second photon initiates the reaction. We compared the reaction and activation dynamics in thermophilic and mesophilic enzymes, and found a reduced speed of product accumulation for the thermophilic enzyme. This effect is explained by a reduced quantum yield of the initial activation process in the thermophilic enzyme, in agreement with an increased conformational rigidity of the thermophilic enzyme at RT. The lifetime of the activated enzyme is long (>24 hrs) and survives the first turnover. The refined biphasic formation rate of the first catalytic intermediate, I675*, $(10.4 \pm 2.1\ ps)^{-1}$ and $(360 \pm 100\ ps)^{-1}$ is derived from a series of systematic measurements. In deuterated thermophilic enzymes, the rates of I675* formation slow down by a factor of 1.5 – 2. This kinetic isotope effect indicates the involvement of protons and that the I675* intermediate is a protonated complex, probably Pchlide*-H+. The quantum yield of the formation of the first catalytic intermediate I675* is estimated to be 0.68±0.11, and of the final reaction product chlorophyllide to be 0.26±0.06.

3.1. Introduction

The efficiency and rate of reactions catalyzed by enzymes may be many orders of magnitudes higher than that of the equivalent reaction in solution[13]. Close positioning of the substrate and cofactor within the catalytic site leads to favorable conditions, but also in other ways enzymes may enhance the catalytic reaction rate: enzymes have been shown to stabilize a transition state conformation by lowering the free energy of activation associated with the reaction by electrostatic interactions[25, 26, 31, 35]. Furthermore, the structural flexibility of proteins is considered to play a central role in the interaction between proteins, interactions between proteins and substrates, allosteric regulation and in catalytic activity. Several enzymes have been reported to have a rest configuration and an active configuration and the dynamic interconversion between such conformational states is important for catalysis. Indeed, the role of conformational changes in explaining the huge catalytic power of enzymes is currently one of the most challenging questions in biology [13, 28-33].

The enzyme protochlorophyllide oxidoreductase (POR), from the family of short-chain alcohol dehydrogenases, catalyses the conversion of protochlorophyllide (Pchlide) into chlorophyllide (Chlide), upon the absorption of light. This is an important regulatory step in chlorophyll biosynthesis and the subsequent assembly of the photosynthetic apparatus. The overexpression of the POR enzyme from the cyanobacterium *Synechocystis* sp. PCC6803 in *E. coli*[47], and from the thermophylic cyanobacterium *Thermosynechococcus elongatus* BP-1[48], has allowed sufficient quantities of pure, water soluble, enzyme to become available for detailed spectroscopic experiments. A detailed review on POR, including studies on POR A and B isoforms from green plants, can be found elsewhere[5, 49, 50], whereas the spectroscopic studies on the isolated enzyme were recently reviewed[51]. We demonstrated earlier that a light-activated conformational change of the protein is necessary to activate catalysis[52]. This makes POR a very important model system to study the relationship between structural changes in enzymes and their functionality. Catalysis is induced by the absorption of light by the Pchlide substrate and, since the enzyme-substrate complex can be pre-formed in the dark, this allows the reaction to be triggered by a short laser pulse and the dynamics to be followed without the interference from substrate and cofactor binding reactions. It is proposed that a conserved Tyr residue donates a proton to the C18 position and a hydride is transferred from the *pro*-S face of the NADPH nicotinamide ring to the C17 position of the Pchlide molecule (see scheme below) [8]. Unfortunately, the structure of POR has not been resolved yet, but a homology model from *Synechocystis* sp. was constructed using a template from the tyrosine-dependent oxidoreductase family[12].

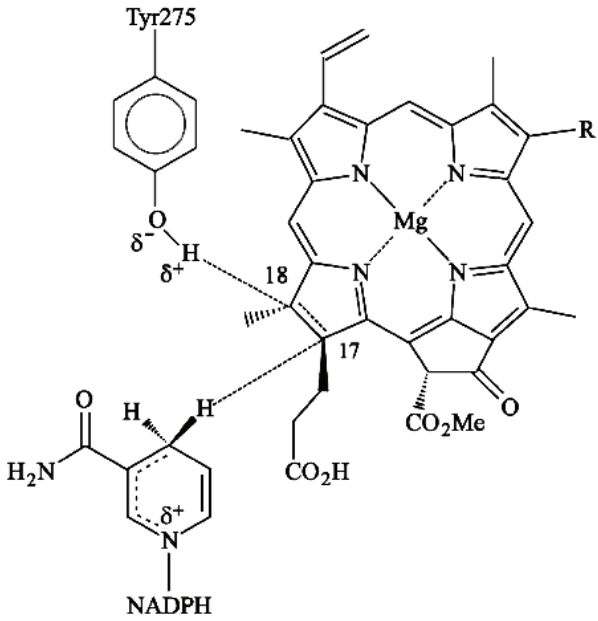

Schematic representation of the POR active site and reaction mechanism.

When bound to the POR:Pchlide:NADPH complex, Pchlide absorbs at 642 nm and fluoresces at 644 nm [18, 47]. By illuminating the POR complex at low temperatures, the reaction can be trapped in an intermediate state and the intermediates can be characterized by CW fluorescence and absorption measurements. Upon increasing the temperature, the reaction can proceed towards the next intermediate. Using this method, several spectroscopic intermediates, prior to the formation of Chlide, were detected, the first being a non-fluorescent intermediate with a broad absorbance band at 696 nm [53]. By using a combination of EPR, ENDOR, and Stark spectroscopies, in conjunction with low temperature absorbance spectroscopy, and isotope labeling this intermediate was shown to be a charge-transfer complex, proposed to result from hydride transfer from the NADPH molecule to the C17 position of Pchlide [54]. This was supported by the observation of a NADPH/NADPD kinetic isotope effect in the rate of formation of the 696 nm intermediate, occurring with a time constant of 0.5 μs [55]. In the same study, a subsequent solvent KIE on a time constant of 40 μs was interpreted as that this step involves the proton transfer from the Tyr donor to the Pchlide molecule. By combining studies of the temperature and isotope dependence of the rate of Pchlide reduction it was shown that both H-transfer reactions proceed by using quantum mechanical tunnelling which is coupled to specific motions

(vibrations) in the protein [55]. Further studies on the role of the bulk solvent on catalysis suggested that solvent-slaved motions control proton tunneling but not hydride tunnelling, implying that a long-range 'dynamic network' from solvent to the enzyme active site facilitates proton transfer [56, 57].

Further intermediates were only formed above the glass transition temperature (200 K), suggesting a role for domain movements and/or reorganization of the protein, and were shown to correspond to a series of ordered product release and cofactor binding events [18, 38, 53, 54], occurring on a millisecond to second timescale. Recently the latter were time-resolved (at room temperature) and release of $NADP^+$ was observed to occur with rates of 1.2 ms^{-1} and 0.2 ms^{-1} and was followed by the binding of NADPH and release of Chlide with a rate constant of 20 s^{-1} [48].

In chapter 2 and in Sytina *et al* [52], we presented a concise description of a study on the thermophilic enzyme, which revealed a highly non-linear light dependency of the final product accumulation, upon increasing illumination. It was shown that with the absorption of one photon, the enzyme complex undergoes a conformational change preparing it for the actual catalysis, occurring upon absorption of a second photon. The first steps in the catalytic reaction were shown to proceed on an ultrafast time-scale, resulting in the formation of the catalytic intermediate I675*, which was proposed to be a strongly hydrogen-bonded complex. The application of analytical methods allowed an estimation of the quantum yield of both the intermediate and the final product, Chlide, and of the activation process.

Conformational changes were shown to play a role in the activation of the enzyme[52]. Therefore, thermal protein motions must contribute to the actual catalytic conversion, involving the proton and hydride transfers. We address this issue here in this chapter by comparing the activation and reaction dynamics of protochlorophyllide oxidoreductase from a mesophilic cyanobacterium, with those from a thermophilic cyanobacterium, *Thermosynechococcus elongatus* BP-1. Thermophilic POR has reduced activity at room temperature[58] and is fully active at 50°C, whereas the mesophilic form of enzyme has optimal activity under RT conditions. Previously, both forms were characterized by using low temperature, steady-state fluorescence techniques[5, 18, 19, 38]. Enzymes have evolved to function optimally at the temperature that their organism survives, and comparing the activity of the two enzymes could reveal which parts of the reaction are determined by temperature and/or protein dynamics[30]. In addition, we compare the reaction dynamics in protiated and deuterated samples, to shed light on the origin of the catalytic intermediate I675*. We further provide a more detailed description of the analytical methods adapted to the non-cyclic nature of the reaction, present the systematic analysis of 15 series of measurements in order to estimate the variation of

kinetic parameters in the different experimental sessions. Finally, we demonstrate the spectroscopic resemblance between a particular subset of POR samples and a previously characterized *in vivo* photoactive 655-nm Pchlide form[4].

3.2. Materials and Methods

3.2.1. Sample

Protochlorophyllide was extracted from *Rhodobacter capsulatus* ZY5, as described previously[38]. POR from the cyanobacteria *Thermosynechococcus elongatus* BP-1 was overproduced in *E. coli* and purified as previously described[19]. The samples contained 0.5 mM Pchlide, 0.5 mM POR and 2.5 mM NADPH in activity buffer (50 mM Tris pH 7.5, 100 mM NaCl, 1% Genapol, 0.1% β-mercaptoethhanol) and were premixed and kept in the dark at all times before the experiment. For the kinetic isotope effect (KIE) measurements POR was deuterated by exchange into a deuterated buffer, containing 50 mM Tris pH 7.5, 100 mM NaCl, 1 mM DTT.

3.2.2. Experimental setup

The laser setup has been described earlier in more detail [28]. The scheme of the visible pump probe setup is shown in figure 3.1. Briefly, the 85-fs pulses of a regenerative Ti:Sa amplifier, operating at 1 kHz, with ~0.8 mJ output pulse energy (Hurricane, Spectra Physics) were used to pump a non-collinear home-built optical amplifier (NOPA) and to generate a white-light (WL) probe beam. The NOPA consisted of two BBO crystals, the first one was pumped by the 800 nm light, in order to generate the second harmonic at 400 nm. The 400 nm pump light together with the white-light seed, generated either using CaF_2 or a sapphire plate (Sa) and a portion of 800 nm beam, were coincided in the second BBO crystal to generate the excitation light, centered either at 475 nm or 640 nm. A 10 nm band pass interference filter at 475 nm or 640 nm was used after the second BBO crystal for output power optimization and in order to spectrally narrow the outcoming pulse. Tilting of the 475 nm filter with respect to the incident beam enabled us to tune the NOPA to 475 nm, which is generally difficult to achieve when sapphire glass is used for generation of the WL seed light. The generated NOPA light then was sent through a delay line which retarded the pump pulse from -15 ps up to 6000 ps with respect to the probe beam.

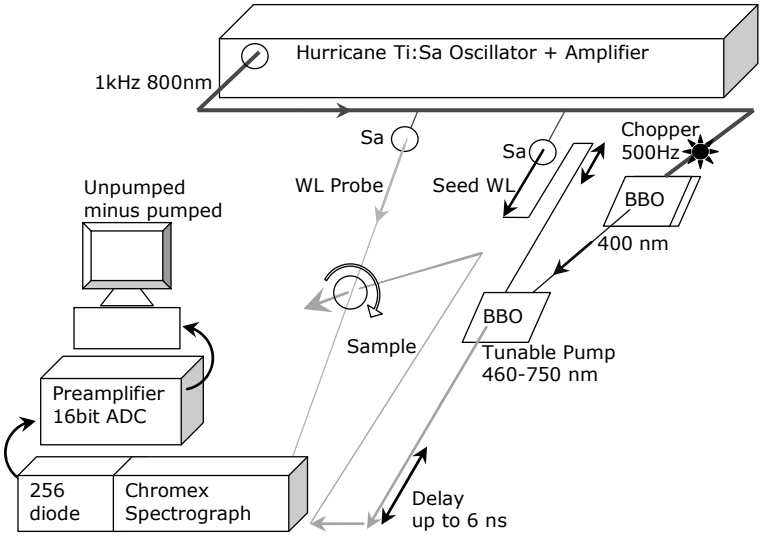

Figure 3.1. Schematic layout of visible pump-probe setup. The arrows denote direction of laser beams.

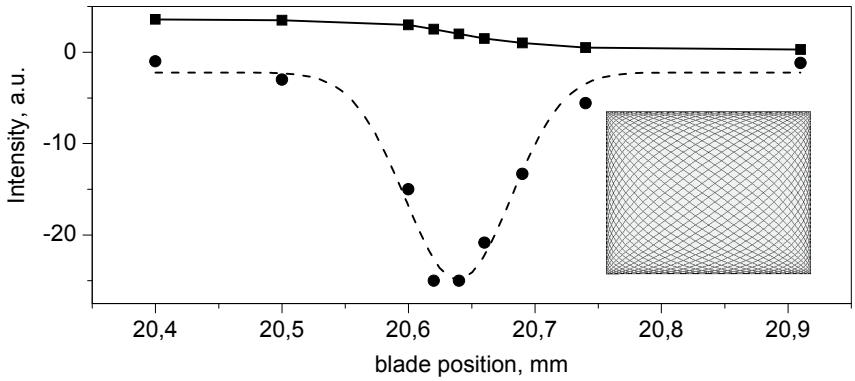

Figure 3.2. Intensity of laser pump beam at 490 nm measured as a function of blade position (squares and solid black line), numerical derivative of the experimental data (circles) and its Gaussian fit (dashed black line). **Inset:** Lissajous pattern.

Excitation of the POR:Pchlide:NADPH complexes was at the red edge of the Soret band (S2–S0 transition) of Pchlide at 475 nm, where the absorption of the product Chlide is

minimal, or at 640 nm which corresponds to the absorption maximum of Pchlide bound to the protein (figure 3.5.A). The excitation energy per laser pulse was 100 nJ in most measurements, focused into a spot of about 160 μm diameter.

The laser pump and probe beams were focused into the sample using lenses, and the beam waist in the focus plane was estimated by measuring the integral light intensity on a photodetector as a function of a screening coordinate. The pump beam in the focus plane was partially blocked by a blade, and light intensity on the photo detector was measured at each position of the blade relative to the beam. A typical curve of the integral signal is shown in figure 3.2. Numerical differentiation of the obtained curve and fitting with a Gaussian function resulted in a FWHM of about 160 μm.

The white-light continuum was generated in a sapphire plate with another part of the 800 nm to monitor the resulting absorption changes in the 500-740 nm spectral region. The polarization of the white-light was at the magic angle with respect to the excitation (54.7^{o}) and was overlapped with the excitation beam in the sample. After passing through the sample, the probe beam was dispersed in a 2-nm resolution spectrograph (Chromex 250IS) and imaged onto a 256-element diode array. The white-light had a 95% pulse-to-pulse stability, as determined from parameters in the acquisition software which were set to a standard deviation window of 3%, resulting in a 90% acceptance for 250 averaged shots. The instrument response function of the setup was about 120 fs, and the collection of the experimental data was performed at 500 Hz repetition rate. The CaF_2 sample cell of 200 μm path length, mounted in a Lissajous sample scanner, was placed in the focus of the two laser beams.

3.2.3. Sample Mover

The Lissajous sample scanner was designed in such a manner as to illuminate a fresh area of the sample with each next laser pump pulse. This design is essential when one deals with non-cyclic reactions, like Pchlide to Chlide conversion by the POR enzyme. In this design, a sample cell continuously moves in a plane perpendicular to the laser pump and probe beams. One cycle of the cell takes approximately one minute, after which the laser pump beam returns to the same sample volume. Since the illumination pattern of the Lissajous scanner looks as depicted in figure 3.2, during one scan some spots are illuminated once and some spots (on the crossing points) are illuminated twice. Choosing a low excitation power, usually not more than 10% of the molecules are being excited per pulse, one is able to observe a gradual accumulation of a photoproduct in the sample, when individually recorded time scans are compared. Variations in the excitation density depended mainly on the fact that we used excitation on the slope of the Soret band at 475 nm with the FWHM of

5 nm, and that a relative shift of a few nm therefore results in a correspondingly larger or smaller excitation density, and on the heterogeneous illumination pattern of the Lissajous scanner, which results in an asynchronous mixture of singly and doubly illuminated spots in one sample scan.

We identify a time-, or sample-scan as a full time-resolved dataset collected within one minute. The very first sample scan is recorded in a sample that has never seen light (assuming that it was prepared and kept in the dark before experiment), the next sample scan is recorded on a sample of which a fraction has seen one photon already, and may absorb a second photon, the third when a fraction of the sample has seen two photons already, and so on. Thus the fraction that has absorbed at least one photon and the fraction that has absorbed a second photon, is gradually increasing in each subsequent sample scan, and, despite some degree of heterogeneity due to the illumination pattern of the Lissajous scanner (figure 3.2), these fractions can be estimated using a kinetic modeling of the recorded time-resolved spectra with a branched kinetic scheme. The procedure will be described further below. Thus, in our experiment, it was absolutely essential to choose an appropriate number of positions on the delay line to cover a time range from -15 ps up to 3000-6000 ps to be recorded within 1 minute. Usually, the number of time points was between 55 and 65. Another aspect is that in order to acquire a data set with sufficient signal to noise ratio, one needs to average an appropriate number of laser pulses for each time point, in our experiment this was 250 shots. Taking into account that the pump repetition rate was 500 Hz, only during 30 seconds from each 60 a sample is illuminated by the laser.

3.2.4. Excitation densities

Besides the target analysis, which enabled us to estimate the excitation density for each dataset individually, as detailed below, there are two experimental methods to determine the fraction of excited molecules in each laser shot. One can calculate the number of excited molecules relative to the total number of molecules in the laser focus, using the following expressions for the number of absorbed photons:

$$N_{photons} = \frac{E - E \cdot 10^{-OD}}{E_{onephoton}}$$

where E is the laser pulse energy (100 nJ in most of experiments), OD is the optical density of the sample at the excitation wavelength (475 nm or 640 nm); The number of molecules is:

$$N_{molecules} = N_A \cdot C \cdot V$$

where N_A is Avogadro's number, and C is the sample concentration:

$$C = \frac{OD}{\varepsilon \cdot path}$$

The concentration can be determined from the absorption of the sample at a wavelength where an extinction coefficient is known, in our case this was 640 nm for Pchlide bound to protein, and 630 nm when Pchlide is unbound, with an extinction coefficient:

$$\varepsilon = 30.1 \frac{L}{mM \cdot cm}$$

V is the illuminated volume, which depends on the focus size, in our case it was 160 μm. Applying these formulas to for example the sample with the absorption spectrum shown as in figure 3.5.A, one obtains an excitation density of 5%.

A similar result can be obtained when the ratio of the total number of photons which the sample absorbs after one sample scan, relative to the total number of molecules in the sample cell is calculated using the following expression:

$$N_{total} = N_{photons} \cdot F \cdot T_{scan} \cdot N_{scans}$$

where F is pump repetition rate, 500 Hz, T_{scan} is the duration of one sample scan, i.e. the total time that the sample cell is illuminated by the pump, usually one scan of the delay line takes 1 minute; N_{scans} is number of scans of a sample. The number of molecules in a sample cell can be estimated in the same manner as given above, where V is the sample volume corresponding to the illuminated area of the entire sample cell, which was 80 μL. Using this method one can obtain an excitation density of 4.5% of molecules which are excited in one sample scan.

Another possibility is to determine the excitation density from a calculation of the ratio of the integral of the bleached signal immediately after photo excitation to the integral of the Q_Y absorption in the steady-state regime, multiplied by 0.5 to account for the contribution of the stimulated emission to the absorption difference signal. This estimate results in ≤5% (slightly depends on the spectral window selected for integration) when 100 nJ power was used.

3.2.5. Averaging

A dataset of time-resolved transient absorption spectra is a N×T matrix, where N is number of wavelength channels, usually 256, and T is number of time points covering a range of –15 to 6000 picoseconds of the delay-line. Since the collection of the data was based on single scan averaging, a few repetitions of the same experiment with fresh sample prepared in the dark was used to obtain sufficient S/N and check reproducibility of the results. A typical amplitude of the Pchlide bleached signal at 640 nm was between 10 to 30 ΔmOD, and averaging 250 shots in the moving sample led to a noise of about 1 ΔmOD, caused by

heterogeneity of the sample, and variation of excitation power due to intrinsic instability of the laser source. The averaging was usually made between the corresponding scans among n data sets with the same calibration of the white-light on and recorded on samples from the same stock preparation, i.e. 1st, 2nd , …. Xth scans could be averaged between n measurements creating one averaged set of scans <1>, <2>...<X>, <X+1>…. Further averaging was done between them if no visible difference in the kinetics and amplitudes was observed.

3.2.6. Kinetic analysis of a non-reversible reaction

Global analysis

The characterization of the light-dependent activation process in the POR enzyme is possible due to a combination of single-photon illumination conditions, and the detailed kinetic modeling of the time-resolved data. Short-scan measurements allow us to control the amount of light the enzyme has seen, or in other words, how often it has cycled through the excited state, and to monitor the concomitant reaction kinetics. In this section we will give a brief description of the global analysis, with further emphasis on the target kinetic modeling.

Global analysis is the basic tool used for the initial characterization of the time resolved dynamics. In our experiments all measurements consisted of a series of consecutive sample scans, and in each sample scan we obtain a time-resolved absorbance difference spectrum. The spectral evolution in the absorbance difference spectrum can be fitted with a sum of sequentially evolving exponential components, in which it is assumed that the time traces collected at all 256 different wavelengths can be described by the same, limited set of exponential decays, and the amplitudes of these exponential decays are estimated, resulting in so-called evolution-associated difference spectra, EADS[40]. A schematic representation of this method is shown in figure 3.3. Instrument response function and lifetimes of each kinetic component are parameters estimated by a fitting algorithm. In the case of POR, the time-resolved spectrum was well fitted with a sum of either three or four exponential components. The quality of the fit is judged by inspection of the singular vectors of the matrix of residuals, which have to be structureless. The instrument response function (IRF) is described by a Gaussian shape, and the white-light dispersion over the spectral range is modeled by a second order polynomial. With increasing lifetimes, and thus decreasing rates in a sequential model, the first EADS decays with the first lifetime and corresponds to the difference spectrum at time zero with an ideal infinitely small IRF. The second EADS is formed with the first lifetime, and decays with the second lifetime. The third EADS is formed with the second lifetime and decays with the

third lifetime, and so on; the final EADS represents the difference spectrum of the longest living species. The EADS may not represent pure species, and they are interpreted as a weighted sum of species-associated difference spectra (SADS).

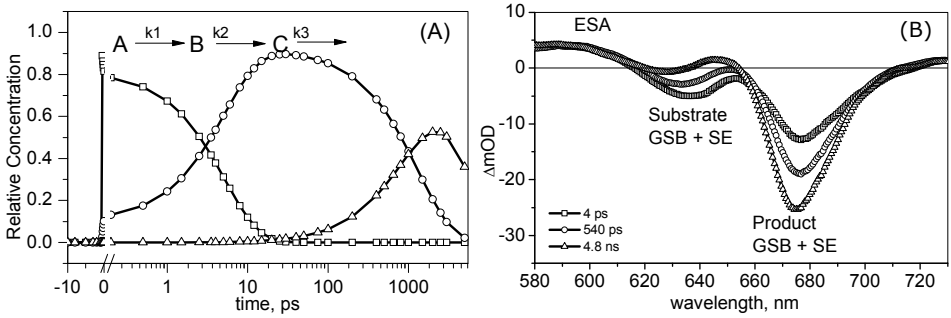

Figure 3.3. (A) Time-dependent concentrations of exponentially decaying excited states A, B, C in the sequential kinetic scheme. **(B)** Evolution-associated difference spectra resulting from a global analysis using a sequential kinetic scheme.

A typical example of EADS, resulting from the global fit of one individual sample scan, is shown in figure 3.3.B. The difference spectrum appearing after absorption of the laser pulse (black line) consists of two negative bands, at 640 nm corresponding to bleached ground state (GS) absorption and stimulated emission (SE) of substrate, and at 675 nm to ground state bleach and SE of the product. The relative intensity of these bands depends on the amount of illumination which the sample has seen prior to this particular scan. In a completely new, dark-kept sample, the band at 675 nm would be absent, having only a positive contribution of excited state absorption (ESA) of the substrate. In the next two steps, after 4 ps and 540 ps, the amplitude of the 640 nm negative band is reduced, while the 675 nm band is increased. Now, the negative signal added to the 675 nm band originates from the SE of the product being formed in this sample scan. Note that this implies that the new product is formed in the excited state. The final spectrum has a lifetime of the order of a few nanoseconds.

The first scan, when no product was formed yet (not shown above, but see results section) shows Pchlide intrinsic excited state dynamics, which required typically three exponential decays to be adequately fitted, with the relevant states denoted Pchlide*I, Pchlide*II and Pchlide*III. Only in subsequent scans, the product state I675* was being formed, and the accumulated Chlide was progressively more excited at t=0 ps. Since the

composite dataset typically consisted of many consecutive scans, a simultaneous target analysis of a series of scans was found to be the best possible way to characterize the gradually changing spectra in more detail.

Target analysis

The structure of the kinetic target model is based on a phenomenological description of the data. Obviously, there are several absorbing and emitting species in the sample solution, with illumination-dependent and time-dependent concentrations, i.e. Pchlide bound to enzyme, Pchlide unbound, Chlide accumulated and intermediate catalytic product being formed in the sample scan. For simplicity, it will be assumed that the fraction of unbound Pchlide is insignificant because the enzyme is mixed with the substrate in 1:1 proportion, with dissociation constant K_d =1.32±0.48 μM for Pchlide binding to POR in the presence of NADPH[58]. The bound population will be divided into a fraction of inactive and active enzyme complexes. It is supposed that the active enzymes can form the I675* intermediate, and inactive enzymes (or unproductive) do not form any product. The fractions of both enzymes are dependent on the amount of illumination, and the unproductive fraction is transformed into productive with increasing illumination or scan number. The consequence of choosing low excitation power is that a significant fraction of enzymes remains inactive in many consecutive sample scans, which allows us to observe the gradual change in sample composition and obtain the required signal-to-noise ratio. The fractions of active and inactive enzymes for each scan, and the total amount of product present after each sample scan are parameters to fit in the target analysis.

In the target analysis, a compartmental scheme is used to describe the concentrations of n_{comp} compartments. Transitions to and from compartments are described by microscopic rate constants, which are not allowed to vary from scan to scan, because physically, transition rates are not light-dependent parameters.

The model that is fitted to each data set is:

$$\psi(\lambda,t) = \sum_{i=1}^{n_{comp}} c_i(t) SADS_i(\lambda),$$

where $c_i(t)$ corresponds to the concentration of the i^{th} compartment, SADSi(λ) is the i^{th} species-associated difference spectrum. The concentrations obey the system of n_{comp} differential equations:

$$\frac{d}{dt} c(t) = Kc(t) + j(t),$$

where K is transfer matrix containing off-diagonal microscopic rate constant θqp from compartment q to compartment p. The diagonal elements contain the intrinsic decay

rates of each compartment. For example, we have used the following transfer matrix to fit the data:

	1	2	3	4	5	6	7	8
1	$-\theta 1$	$\theta 1$	.	.	.	.	.	.
2	.	$-\theta 2$	$\theta 2$	.	.	.	.	.
3	.	.	$\theta 3$	.	.	.	.	.
4	.	.	.	$-(\theta 1+\theta 5)$	$\theta 1$	.	$\theta 5$	.
5	.	.	.	.	$-(\theta 2+\theta 6)$	$\theta 2$	$\theta 6$	.
6	.	.	.	.	.	$-(\theta 3+\theta 7)$	$\theta 7$	.
7	.	.	.	.	.	.	$-\theta 4$	.
8	.	.	.	.	.	.	.	$-\theta 4$

The eight compartments are depicted in figure 3.4. The input to the compartments is:

$$j(t) = IRF(t)[\chi_1 \quad 0 \quad 0 \quad \chi_2 \quad 0 \quad 0 \quad 0 \quad \chi_3]^T,$$

here χ_1, χ_2, χ_3 are the fractions of inactive enzymes, active enzymes and accumulated Chlide respectively, thus it is requered that the sum of all fractions is $\chi_1+\chi_2+\chi_3$=1 in each sample scan.

The kinetic scheme and corresponding concentrations of spectral compartments used to fit the POR dynamics are shown in figure 3.4. The 4→5→6 sequential branch (figure 3.4.A) represents the evolution of active enzymes which have the possibility to form the intermediate photoproduct I675* from each of the Pchlide*I, Pchlide*II and Pchlide*III excited states, and the 1→2→3 sequential branch represents inactive enzymes which show only Pchlide* photochemistry and do not form I675*. We assume that the Pchlide* photochemistry is intrinsic to its excited state and therefore is not dependent on the activation state of the protein. The direct excitation of Chlide accumulated in previous scans is taken into account by including a compartment $Chlide_{accum}$*. The assumption that this SADS does not evolve is supported by the observation of only a minor spectral evolution in an almost completely converted sample (data not shown).

A number of spectral constraints were implemented in the model. Substrate bound to active enzyme and substrate bound to inactive enzyme were set to be spectrally undistinguishable, i.e. $SADS_1$=$SADS_4$, $SADS_2$= $SADS_5$, $SADS_3$= $SADS_6$, thus the total number of SADS was reduced from 8 to 5. In different cases the spectral evolution of inactive/active Pchlide* could be fitted reasonably well by only one or two spectra. The simultaneous fit of multiple datasets is the option of choice in this model. The described model will be referred to *free fractional model 1*.

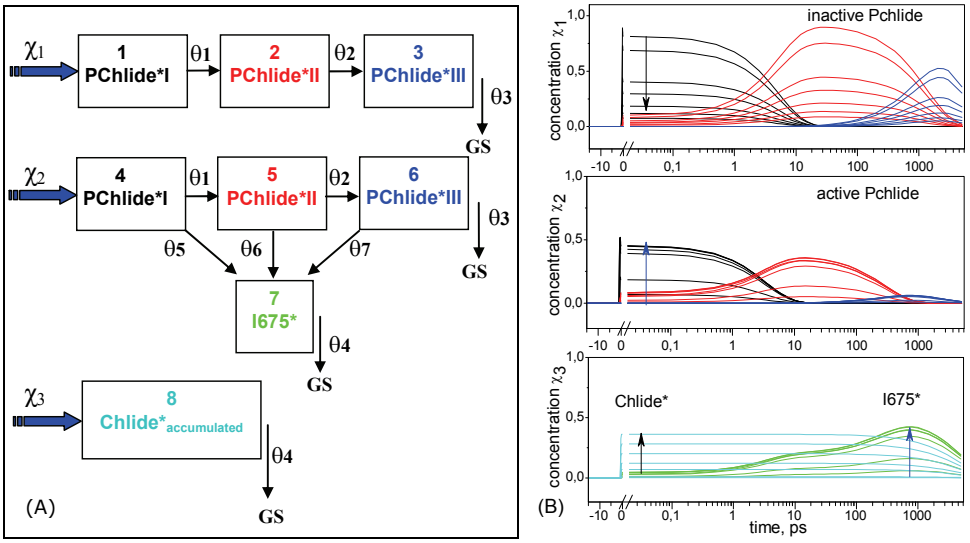

Figure 3.4. Target analysis of the illumination-dependent POR pump-probe datasets. **(A)** kinetic scheme for active and inactive enzymes. The transition rates estimated for all datasets are shown in table 3.1. **(B)** Time-dependent concentrations of compartments, multiple curves correspond to are concentration profiles for increasing scan numbers. Solid arrows show decrease in concentration of inactive enzymes (top black, red, blue) with scan number due to transformation into active enzymes (middle black, red, blue), which are transformed into I675* (green) with increasing scan numbers. The amount of Chlide*accumulated (cyan) increases with scan number. The amount of active enzymes and I675* (blue arrows) initially increases, and further it decreases with increasing illumination.

This model has a large number of free parameters, namely the fractions χ_1, χ_2, χ_3 for each scan and rate constants $\theta_1 - \theta_7$. Therefore, in order to reduce the number of parameters, an analytical dependence of the fractions on the number of scans was introduced. The dependence of the freely fitted fractions resembled curves that described the populations of once, or twice excited enzymes, assuming quite reasonable excitation rates (or rather excitation density per pulse). We therefore reduced the free fraction parameters to two, with k_1 (effective excitation density, in photons per molecule) and k_2, by solving the rate equations for the consecutive reaction mechanism $\chi_1 \rightarrow \chi_2 \rightarrow \chi_3$ with excitation rates k_1 and k_2. For simplicity, in first order we identify one scan as illumination by one laser pulse, with excitation density k_1.

$$\frac{d\chi_1}{dN} = -k_1 \cdot \chi_1$$

$$\frac{d\chi_2}{dN} = k_1\chi_1 - k_2\chi_2$$

$$\chi_3 = 1 - \chi_1 - \chi_2$$

with χ_1 – fraction of inactive enzymes, χ_2 – fraction of active enzymes, χ_3 – product Chlide, k_1 – effective excitation density, $k_2 = k_1 \cdot Q$, Q is quantum yield of Chlide formation, N indicates scan number. Further in the text, this model will be referred to as *analytical or amplitude model 2*. As a result, by measuring the dynamics on a picoseconds time scale and the concentrations of the different populations as a function of the illumination history, we independently determine the quantum yield of I675* intermediate product and the yield of the final product Chlide.

3.3. Results

3.3.1. Spectroscopic signatures of chlorophyllide formation

The visible absorption spectrum of the POR:Pchlide:NADPH complex in the 400-800 nm region is determined by the electronic transitions of the chromophore, either bound or unbound to the protein. A typical absorption spectrum displays the Soret band peaking at 444 nm, and the Q_X and Q_Y bands of substrate and product (figure 3.5.A). The band belonging to the unbound substrate, i.e. free Pchlide in solution, is usually found at 630 nm, the effect of binding to the protein shifts this band towards 640 nm. The relative intensity of the 640 nm band with respect to that at 630 nm is directly proportional to the fraction of bound substrate, assuming that the extinction coefficients of bound and unbound Pchlide are equal. A sample solution containing enzyme, substrate and cofactor that has never seen any light does not have any features in the absorption spectrum in the region above 650 nm. Upon visible light illumination the absorption spectrum is modified due to the reduction of Pchlide into Chlide. A distinct Q_Y band of Chlide appears at 670-675 nm while Pchlide absorption at 640 nm is reduced.

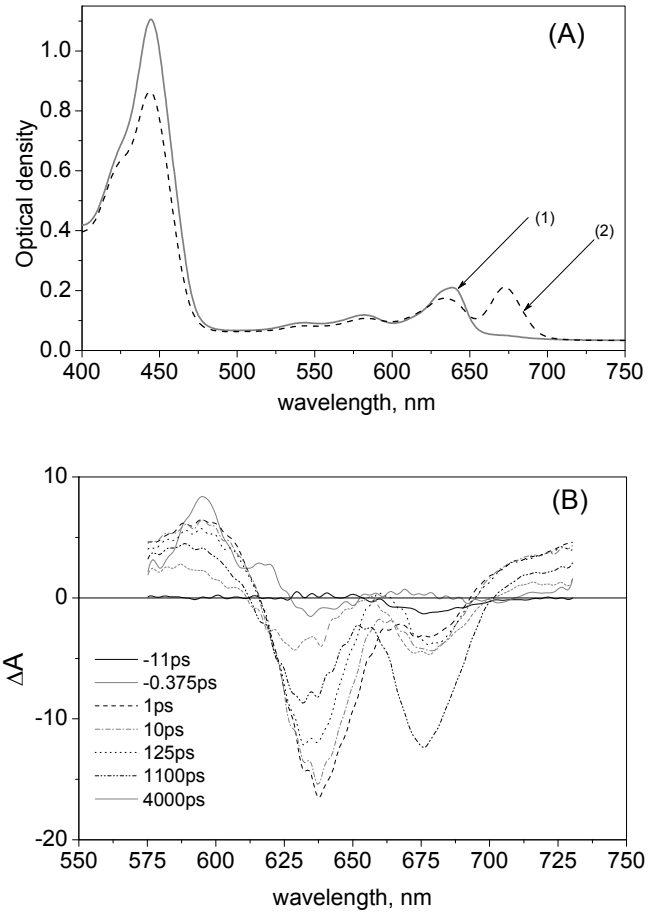

Figure 3.5. (A) Absorption spectrum of POR:Pchlide:NADPH solution measured in 1 mm cell before (1) and after illumination (2). **(B)** Selection of the transient absorption spectra at -11, -0.375 ps before excitation and 1, 10, 125, 1100, and 4000 ps after laser pulse corresponding to scans 7-12. The data is not dispersion corrected.

3.3.2. Kinetics in mesophilic and thermophilic enzymes

Ultrafast time–resolved pump-probe absorption difference spectra of POR from mesophilic *Synechosystis* PCC6803 and thermophilic *Thermosynechococcus* BP-1 enzyme were recorded between -10 ps and 2.5 or 6 ns, in subsequent scans. The experimental procedure of these measurements can be schematically represented by protocol 1 in figure 3.9. In figure 3.5.B a selection of the recorded absorption difference spectra are shown. Before

laser excitation, at -11 ps and partly at -0.375 ps, there is no differential absorption, at 1 ps after excitation (blue line) two negative bands appear at 640 nm and 675-680 nm, which correspond to GS bleaches and SE from Pchlide and Chlide. At later delay times, the amplitude of the 640 nm band decreases, whereas the band at 675-680 nm first increases, and after 4000 ps also decreases in amplitude.

The experiment with thermophilic and mesophilic enzymes taken from two different batches was repeated twice. In the first (high-power) experiment we had 5 mesophilic POR samples taken from one batch, and 4 thermophilic samples from one batch, used a laser pump energy of 200 nJ per laser pulse, and acquired in total 10 sample scans per sample, where the time for collecting one scan was more than 1 minute. The data were divided in three sets, scans 1 and 2, scans 3-6 and scans 7-10, and subjected each to a global analysis. The results of these analyses in the form of EADS are shown in figure 3.6 A , B.

In the second (low-power) experiment, with 3 mesophilic and 5 thermophilic samples, we reduced the laser excitation power to 100 nJ and acquired less time points, 48 in order to reduce the acquisition time. This way we had better controlled illumination conditions, in which a single sample scan corresponds to illumination by one laser pulse. This dataset consisted of a larger number of sample scans, 55, which were divided into several separate consecutive periods and averaged to improve the signal-to-noise ratio. In figure 3.6.C, D the result of the global fitting of this experiment is shown. The data on thermophilic POR from this experiment were presented earlier in chapter 2.

The EADS result from the fit of one full dataset to a minimal kinetic model consisting of four exponentially decaying components with increasing lifetimes. The negative bands in the EADS in the 580-650 nm region are composed of bleached GS absorption and SE from the Pchlide either bound or unbound to the enzyme, and the 650-725 nm region consists of the SE signal from the newly formed product in the excited state, also the signal of bleached GS absorption and SE of Chlide that had been accumulated in previous sample scans. All positive bands arise from ESA to higher electronic energy levels.

Although both enzymes show similar behavior, the thermophilic POR has a slightly reduced speed of product accumulation with increasing number of scans. In the first experiment the mesophilic enzyme shows the appearance of a band at 670 nm already after 3 ps in the first round (top graph 3.6.A), while in the thermophilic it appears after 33 ps (top graph 3.6.B). In the second and third rounds, the first spectra of mesophilic POR show significant signal of directly excited Chlide, whereas thermophilic enzyme does not (middle and bottom graphs 3.6.A, B). Also the amplitude of the excited Pchlide signal at 640 nm is getting smaller with increasing illumination, in contrast, the amplitude of the product signal at 670-675 nm is increasing.

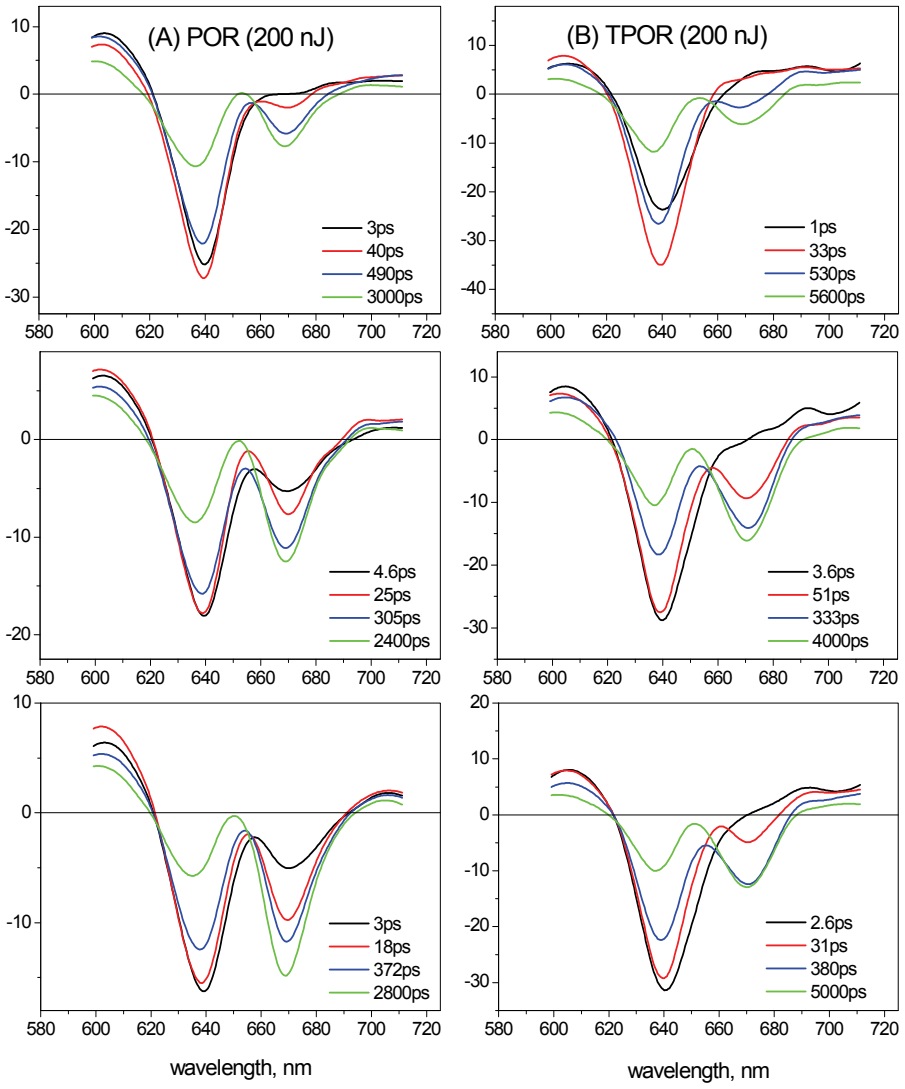

Figure 3.6. EADS resulting from the global analysis of the high-power transient absorptions recorded in **(A)** mesophilic POR and **(B)** in thermophilic POR. The top graphs correspond to 1-2 sample scans, middle to scans 3-6, bottom to scans 7-10.

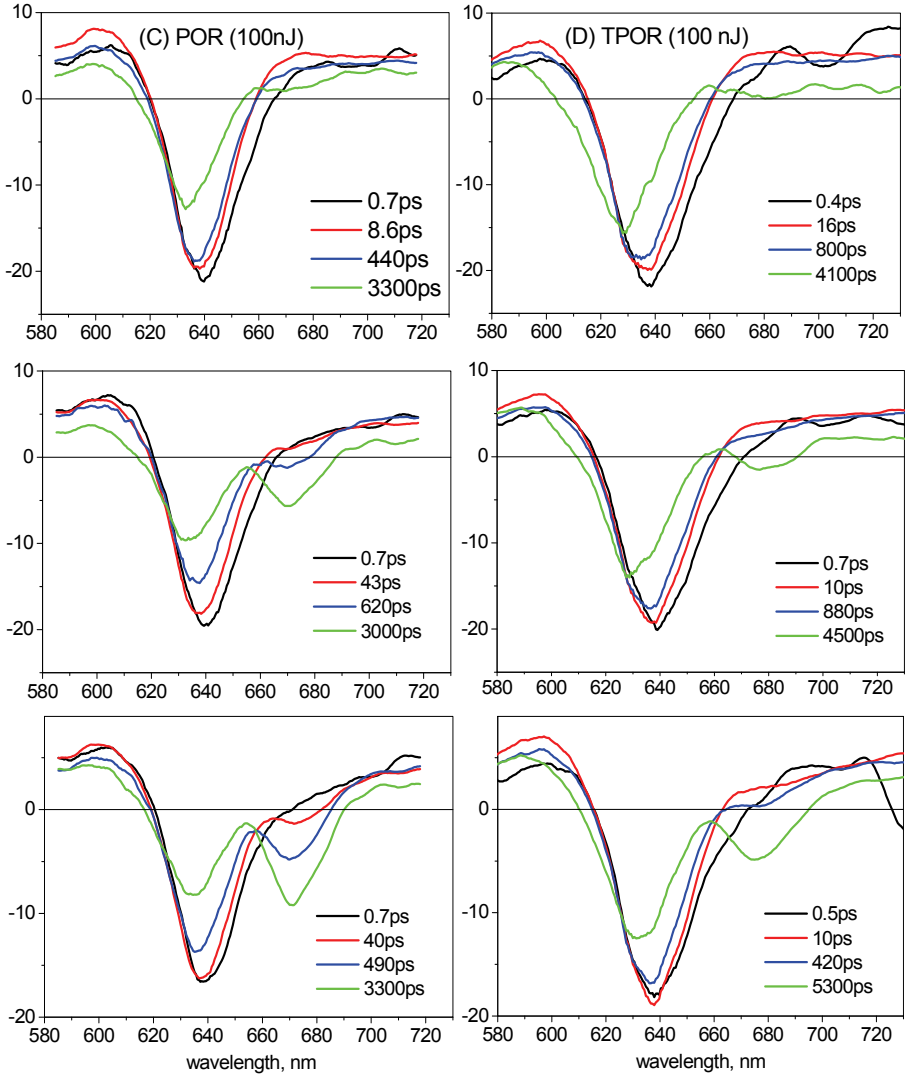

Figure 3.6. EADS resulting from the global analysis of the low-power transient absorptions recorded in **(C)** mesophilic POR and **(D)** thermophilic POR. The top graphs represent scans 1-2, middle 3-6, bottom 7-12. The analysis presented in chapter 2 is based on the data in panel D, whereas the data in panel C has not been analyzed previously.

In the low-power experiment (figure 3.6.C, D) the same effect is observed. In the first round, in the 1st and 2nd scans, both enzymes do not show the 670 nm negative signal because of reduced illumination as compared to the previous experiment (top graphs 3.6.C, D). But, in the second and third rounds, in the mesophilic form, the 675 nm negative signal appears after 43 ps and 0.7 ps respectively and is more intense, whereas in the thermophilic sample the distinct band at 675 nm appears only in the third round after 420 ps. Also in thermophilic POR, the amount of bleach at 640 nm stays more or less identical in all three groups of scans, whereas in mesophilic POR there is a reduction of the 640 nm bleach from -22 ΔmOD to -17 ΔmOD, indicative of more efficient conversion of Pchlide into Chlide.

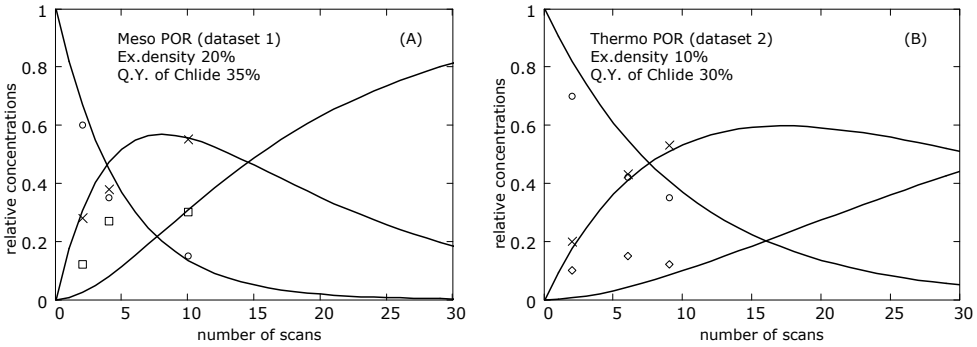

Figure 3.7. Fractions (open circles) as a function of scan number obtained in fitting the data from the high-power experiment with fractional kinetic model 1, and simulation (solid lines) using sequential scheme inactive→active→Chlide according to amplitude model 2. **(A)** mesophilic enzymes **(B)** thermophilic enzymes.

To characterize quantitatively the observed differences in the yield of product formation in the two forms of the enzyme, the data from all measurements were fitted with the kinetic models described in the Material and Methods. As a lower number of scans were recorded in the first experiment, the better alternative was to fit this dataset to the free fractional model 1. It was reasonable to assume that the fraction of active thermophilic enzymes after two sample scans is smaller than in the mesophilic POR, because in the first round we observed more positive signals in the 675 nm region in the thermophilic POR and less negative signal corresponding to I675* (top graph figure 3.6.B). Initially, this assumption was used for a rough estimation of SADS and fractions in all 6 datasets from the first experiment. The initially found fractions in the target fit were then used to simulate possible concentration profiles for inactive, active enzymes and Chlide product in each sample scan, using analytical amplitude model 2 for concentrations. In the next step, the

analytically obtained values were given as starting parameters to model 1 for final optimization. It turned out that the data could be best fitted when the excitation density, k_1, in the simulation corresponds to 20% in the mesophilic enzyme, and 10% in the thermophilic enzyme, despite the fact that in the experiment identical pulse energies of 200 nJ per pulse were used for both enzymes. The rates in the inactive branch, as well as in the active, were found to be similar for both enzymes, and any variation is likely to reflect a freedom in the fitting due to noise and the limited number of sample scans, they are reported in table 3.1 for datasets 1, 2. The results in figure 3.7 demonstrate that the simulated curves for inactive and active enzymes overlap reasonably well with the fractions obtained in the target fit.

The data from the low-power experiment had a larger number of scans and the amplitude model 2 could be directly applied (figure 3.8.A, B). Similar to the previous case, the best quality of SADS and fit of the kinetics was achieved with the excitation density in the mesophilic enzyme lower than in the thermophilic enzyme, i.e. 8% vs 4% respectively, whereas the lifetimes of SADS were found to be similar in both enzymes. When, as a test, the excitation density was assumed to be identical in both enzymes, we could not achieve the same quality of fit. The quantitative parameters found in the two experiments are summarized in table 3.1, datasets 1,2,3,4. The applicability of the target analysis is judged from the interpretability of the SADS.

The SADS estimated with analytical model 2 (figure 3.8.C, D) of the Pchlide*I, Pchlide*II and Pchlide*III excited states are flat in the 670-720 nm region and represent excited state absorptions of Pchlide. The spectrum resolved for the I675* state (green) has negative bands around 675 nm and 640 nm, consistent with stimulated emission from I675* and bleached absorbance of Pchlide. The amplitude of the 640 nm band in the I675* spectrum (green), relative to that of Pchlide*I (black) is consistent with the contribution of ground state bleach (GSB) only in the former, and of both GSB and SE in the Pchlide*I spectrum. The quantum yield of I675* formation can be calculated from the reaction rates, which results in 0.85 and 0.84 for both enzymes (table 3.1, datasets 3, 4). The amplitude of the SE signal at 675 nm is about two times larger than the Pchlide bleach in the I675* spectrum. This most likely represents an increase in the chlorin extinction coefficient, going from Pchlide to the I675* state. Finally, the spectrum of the state $Chlide_{accum}$* (cyan) is consistent with directly excited Chlide, which is formed in previous illuminations of the sample.

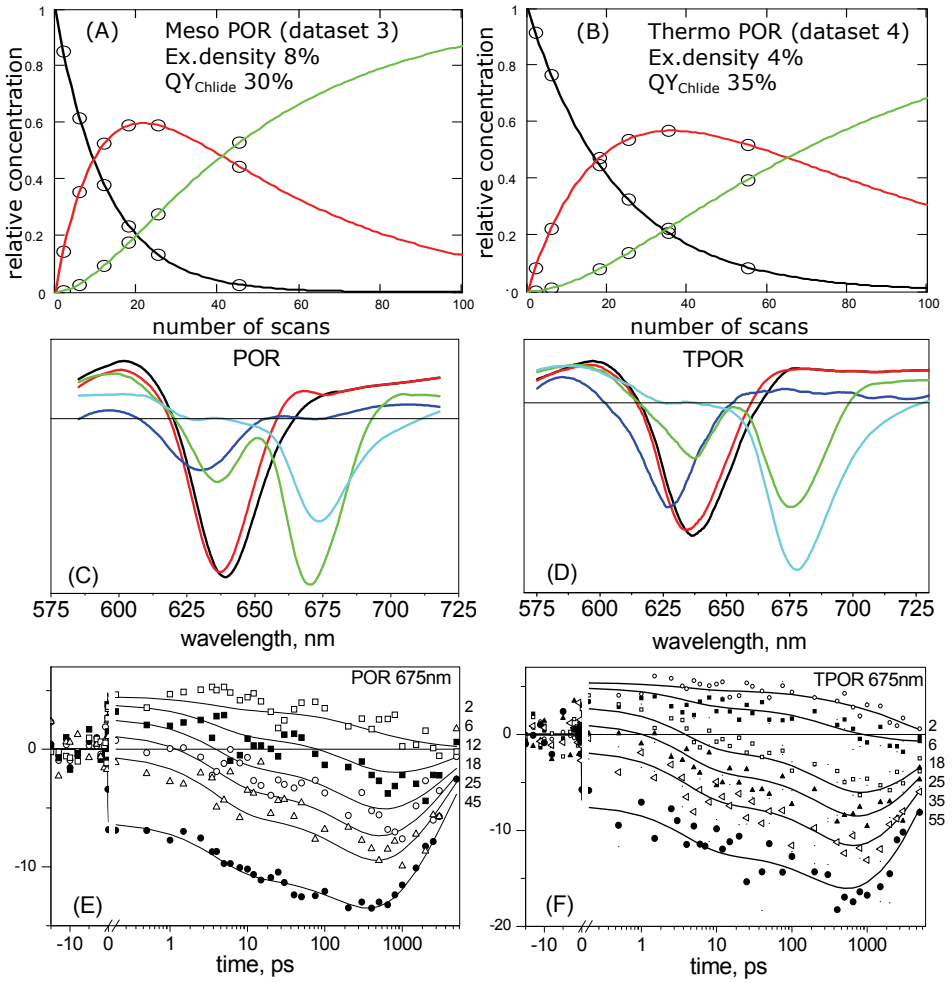

Figure 3.8. (A), (B) Fractions (open circles) obtained in amplitude model 2 for data from the low power experiment. Simulation (solid lines) obtained using sequential scheme inactive(black) → active (red) → $Chlide_{accumulated}$ (green). **(C), (D)** SADS obtained in analytical model 2. The black, red, blue lines correspond to the Pchlide*I, Pchlide*II, Pchlide*III states (compartments 1–6), green spectra correspond to bleached Pchlide band at 640 nm and SE of I675* state (compartment 7), cyan spectra – directly excited Chlide (compartment 8). **(E), (F)** The 675 nm TA data and target fit for increasing sample scans. Note that the 6th sample scan in both enzymes show the appearance of distinct negative signal in mesophilic POR after 100 ps but only after 500 ps in thermophilic POR.

In the time-traces of consecutive scans one can see that the negative signal from the intermediate product I675* is not present in the initial 1st and 2nd sample scan (figure 3.8.E, F) in both PORs. The initial positive signal is due to excited state absorption of Pchlide*, while in the next scans the kinetics change dramatically and the earliest appearance of the negative signal is observed after 100 ps in mesophilic POR, and 500 ps in thermophilic POR. In the following scans, the negative offset at 0 ps is defined by the sum of excited state absorption of Pchlide* and by the amplitude of the GS bleach and SE of accumulated Chlide* directly excited by laser pulse.

In the global analysis, and by visual comparison of traces of transient absorption, there is obviously a later appearance of I675* signal in thermophilic POR, as compared to mesophilic POR (compare first and second traces in figure 3.8.E, F). It turns out that in the target analysis the excitation rate is the only parameter capable of capturing the difference. Note that there is a minor difference in estimation of rate parameters θ5, θ6 between datasets 1 and 2, and between datasets 3 and 4 (table 3.1). In the analysis of both independent experiments, the excitation rate in the mesophilic enzyme is found to be twice of that of the thermophilic enzyme, even though the illumination conditions and optical density were identical for both samples. It is important to realize that the excitation rate k_1 for the activation step is in fact a convoluted number, determined by the excitation density per pulse, the number of laser pulses per scan per sample area and the quantum yield of activation. We will return to this point in the discussion. The effective quantum yield of Chlide formation is similar for both enzymes, 30 and 35%.

Figure 3.9. Schematic representation of different experimental protocols. The block "Dark POR" indicates a sample containing either thermophilic or mesophilic enzyme, substrate Pchlide and NADPH at concentration given in the Materials and methods section. The number of fresh samples used in protocols is shown in table 3.1 and indicated as parameter S. The block "Abs. spectrum" in protocol 1 indicates recording of the visible absorption spectrum, however it has been done not for all samples, therefore shown in dashed line. The block "N scans" indicates recording of N consecutive sample scans with laser illumination. The block "Incubation time T" indicates that the sample is kept in the dark during time T, varied between 30-60 minutes. The block "CW" indicates illumination of a sample with a CW tungsten lamp.

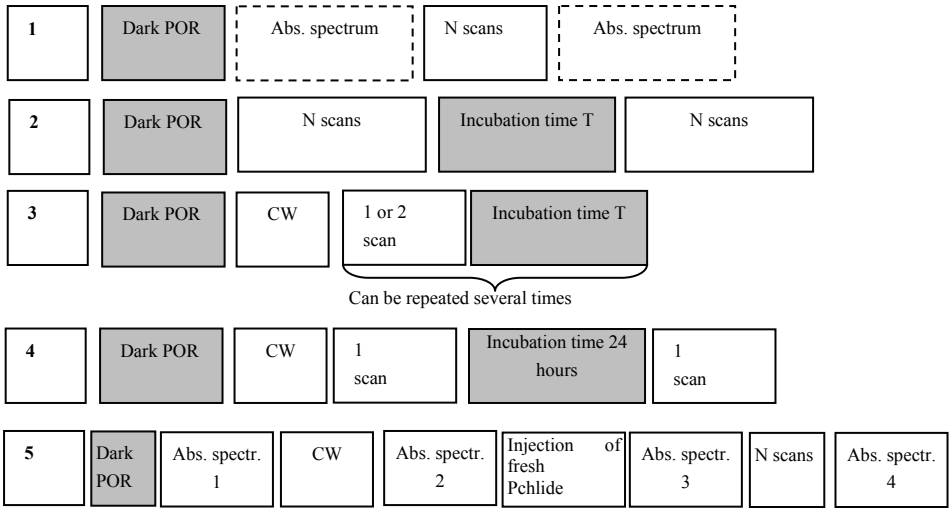

Table 3.1. The lifetimes in picoseconds, $\theta 1^{-1}$, $\theta 2^{-1}$, $\theta 3^{-1}$, $\theta 4^{-1}$, for spectral evolutions of compartments and $\theta 5^{-1}$, $\theta 6^{-1}$ for I675* formation estimated in the target analysis of different experimental sessions. The parameter $\theta 7^{-1}$ was estimated in the models as 0 and not shown in table. Unless indicated otherwise, the numbers refer to thermophilic POR. Parameter λ denotes excitation wavelength in nanometers, used in each experimental session. Parameter **D** indicates the number of sub-datasets, in which the series of N scans in **S** fresh sample preparations was devided. Parameter **N** is total number of scans acquired in each experimental session; **CW** indicates an illumination with the tungsten lamp. Parameter **P** indicates experimental protocol used in each experimental session, the protocol schemes a shown in figure 3.9. Parameter k_1 is excitation rate for the Inactive→Active mechanism, estimated in analytical model 2. The (s) mark in datasets 1 and 2 indicates that parameters k_1, k_2 and QY of Chlide were obtained in simulation. The expression for quantum yield QY of I675* formation is given in Discussion section 3.4.3. Parameter QY of Chlide is calculated as k_2/k_1, where k_2 is derived from analytical model 2 for the Active → Product mechanism.

n	Sample	λ	P	S	D	N	$\theta 1^{-1}$	$\theta 2^{-1}$	$\theta 3^{-1}$	$\theta 4^{-1}$	$\theta 5^{-1}$	$\theta 6^{-1}$	k_1	**QY of I675***	**QY of Chlide, k_2 / k_1**
Measurements on different days															
1	MesoPOR, NADPH, H_2O	475	1	5	3	10	5.3	180	1900	2930	11	322	0.2 (s)	0.57	0.35 (s)
2	NADPH, H_2O	475	1	4	3	10	7	170	2700	4500	10	500	0.1 (s)	0.56	0.3 (s)
3	Meso POR NADPH, H_2O	475	1	6	6	55	7	750	3900	3400	9	263	0.08	0.85	0.3
4	NADPH, H_2O	475	1	6	6	55+CW	7.5	650	5100	4500	8	289	0.04	0.84	0.35
5	NADPH, H_2O	475	1	1	15	31	7.8	600	8400	3796	12	378	0.2	0.76	0.20
6	NADPH, H_2O	475	2	4	17	25	4.3	270	2700	1200	11	350	0.12	0.59	0.30
7	NADPH, H_2O	475	2	2	15	34	4.4	240	1800	1800	8	578	0.18	0.54	0.30
8	NADPH, H_2O	640	2	1	15	61	6	460	2660	2600	12	462	0.05	0.66	0.20
9	NADPH, H_2O	640	2	1	15	59	6.2	340	1500	2300	15	370	0.13	0.63	0.15
10	NADPH, H_2O	640	2	1	15	59	5.9	710	4000	2000	9	357	0.06	0.79	0.20
11	NADPH, H_2O	475	5	1	17	CW+25	6	390	2300	1600	9	206	--	0.79	--
12	NADPH, H_2O	475	5	1	17	CW+70	5.7	120	2700	1400	9	256	--	0.57	--
13	NADPH, H_2O	475	5	1	17	CW+20	4.8	190	3000	1700	8	269	--	0.63	--
14	NADPD, H_2O	475	1	2	15	67	4.8	180	1900	2400	5	486	0.07	0.51	0.30
15	NADPD, H_2O	475	1	1	15	47	3.9	120	1800	2200	8	373	0.035	0.47	0.34
	Mean						**6**	**350**	**3100**	**2500**	**10**	**360**	**0.10**	**0.68**	**0.26**
	St.dev.						**1**	**200**	**1700**	**1050**	**2**	**100**	**0.06**	**0.11**	**0.06**
The KIE measurements on the same day, parameters obtained in simultaneous target analysis															
16	NADPH, H_2O	475	4	3	3	CW+1	7.5	230	2900	2120	8.4	149	-	0.79	-
17	NADPH, D_2O	475	4	3	3	CW+1	7.5	230	2900	2120	17	212	-	0.66	-

Figure 3.10 (next page). **Left column:** SADS estimated in the target analysis (amplitude model 2). **Middle column:** relative concentrations as a function of scan number (analytical amplitude model 2). **Right column:** relative concentrations obtained in free fractional model 1. In fraction fits black lines are unproductive enzymes, red lines are productive enzymes, cyan lines are accumulated Chlide. The time constants and quantum yield parameters for each dataset are shown in table 3.1.

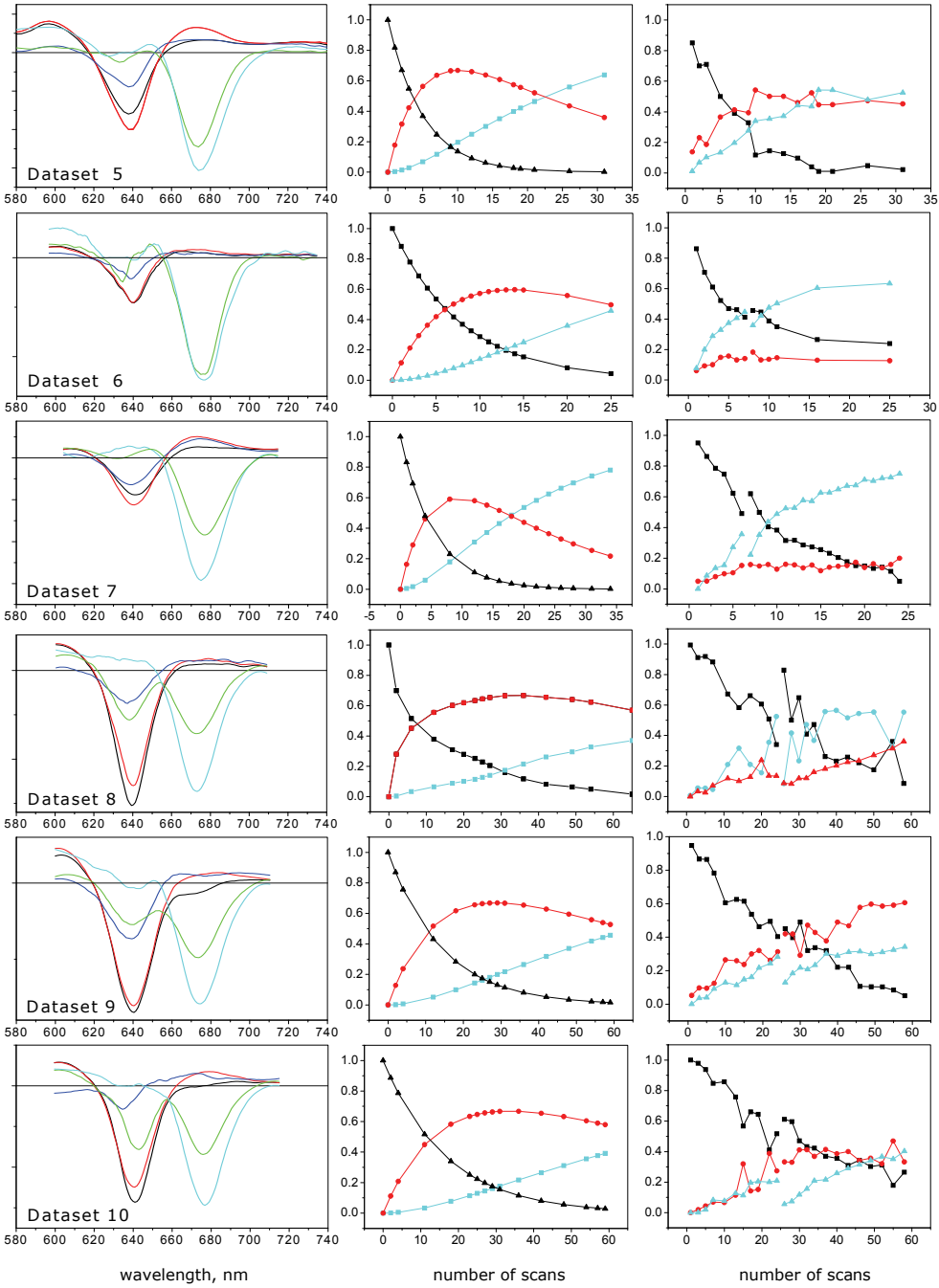
Dataset 5
Dataset 6
Dataset 7
Dataset 8
Dataset 9
Dataset 10
wavelength, nm
number of scans
number of scans

3.3.3. Dynamics upon excitation at 475 nm or 640 nm

There is a variation in intrinsic Pchlide* dynamics (black, red, blue SADS) when either 475 nm or 640 nm excitation is used. In the case of blue excitation, the initial black spectrum evolves into a more intense red spectrum (figure 3.10 datasets 5,6,7), whereas a gradual decrease from black to red is observed upon direct excitation of the Q_Y at 640 nm (figure 3.10, datasets 8, 9, 10). The effect of emission gain upon blue excitation has also been observed in neat Pchlide solutions and will be described in chapter 5 in more detail, where it is shown to be related to the relaxation from the S2 to the S1 excited state.

3.3.4. Lifetime of the POR activated state

In section 3.3.2 and chapter 2, we showed quantitatively that the light-driven catalytic reduction of Pchlide by the POR enzyme is a two-photon process. Absorption of the first photon turns the enzyme to the "On" state, which is likely to involve a readjustment of the active site, as shown in chapter 2. The conformational optimization enables the next catalytic step to occur upon absorption of the second photon. In order to test the lifetime of the activated POR:Pchlide:NADPH complex, i.e. the lifetime of the active conformation, we performed additional transient absorption experiments.

In a first attempt to determine the lifetime of activated complexes, we tested whether there was decay in the concentration of activated complexes when a sample was kept in the dark for a period of 30-60 minutes. The experimental procedure can be schematically represented by protocol 2 in figure 3.9. The fractions estimated by model 1 for these measurements are shown in figure 3.10 (right column, datasets 6-10), where a distinct gap is seen in all fractions. Before the dark period, there is a continuous growth in the amount of produced Chlide, and a decrease in the fraction of inactive enzymes. After the dark period, the amount of inactive enzymes has increased by about 10%, consistent with a decay of the activated state. However, the amount of Chlide is also significantly reduced by about 10%, therefore diffusion processes in the sample during the dark period are a more likely reason for this discontinuity. The design of the sample cell does not allow illumination of the entire sample volume loaded into the cell, thus there is always a fraction of the sample volume that has not seen any light during many scans (inset in figure 3.11).

We next performed an experiment to reveal the lifetime of the active conformation, which has been briefly described in chapter 2 already. In the experiment, in order to obtain *homogeneous* illumination, a reaction mix of protein, substrate and cofactor was prepared in the dark with concentrations of 0.5 mM of thermophilic POR, 0.5 mM Pchlide and 3 mM NADPH and illuminated by a CW 40 W tungsten lamp being placed in a 1 mm path quarts

cuvette 50 cm away from the lamp, no heat or spectral filter were used. The pre-illumination time was 30 seconds, which was long enough to get a large fraction of activated complexes in the sample. The experimental procedure corresponds to protocol 3 in figure 3.9.

After the CW illumination, 12 transient absorption measurements in the 480-730 nm region with dark breaks of different lengths between each next 2 scans were recorded. The total time between activation of the complex by pre-illumination and last recorded scan was about 7 hours. Figure S4 in chapter 2 illustrates the effect of a dark interval of in total of 7 hours on the TA kinetics of the POR sample. The traces of transient absorption recorded at 670 nm were normalized on the amount of initially excited Chlide, i.e. on the amplitude of the signal at 0 ps delay. Thus, the difference between the kinetics in the scan recorded after pre-illumination and the scan recorded after 7 hours reflects the effect of the dark incubation, the amount of Chlide produced per laser pulse (per scan) is reduced. The decrease in the amount of Chlide produced per laser pulse between the first and last sample scan is about 30%. A quantitative estimate was made by calculation of the differences in areas under the two curves after subtraction of the contribution of directly excited Chlide. The estimated relative decay of Chlide production per laser pulse as a function of the length of the dark intervals between scans is shown in figure S4 in chapter 2. The data points can be fitted by an exponentially decaying function $f(t) = e^{-t/T}$, where T is 19 hours.

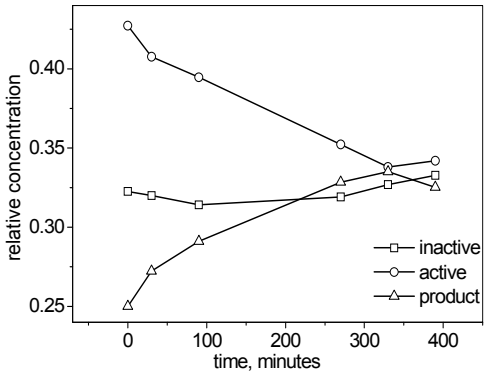

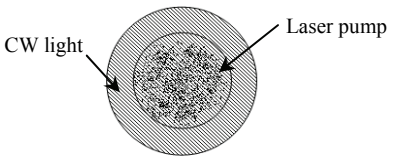

Schematic representation of inhomogeneity of illumination in sample cell. The area confined in the outer circle is homogeneously CW illuminated before the TA experiment, the area confined in the inner circle received additional laser illumination in the following 12 test scans.

Figure 3.11. The fractions of unproductive and productive enzymes and Chlide present in the single sample scans as a function of the dark incubation time, obtained by fitting the data with fractional model 1. The fractions correspond to measurements in the same sample recorded at 0, 30, 90, 270, 330, 390 minutes after initial CW illumination.

Therefore, there is an apparent change in the kinetics after 7 hours in the dark. However, fitting the data with fractional model 1, results in very little increase of the unproductive fraction, from 32% right after CW illumination to 33% after 7 hours without illumination (figure 3.11). One would have expected at least an increase of the inactive fraction proportionally to the reduction in Chlide formation, i.e. of about 30%. The productive fraction drops from 47% to 40%, and the amount of Chlide increases from 25% right after CW illumination to 30% after 7 hours. Most likely, the decrease in productive fraction is due to conversion into Chlide but not due to decay of the active conformation, because it does not give rise to an increase in the amount of unproductive enzyme. The conversion into Chlide is an effect of the total of 12 scans that were recorded in this experiment. Thus, from this experiment we can only tentatively conclude that the activated state of the enzyme has a long lifetime.

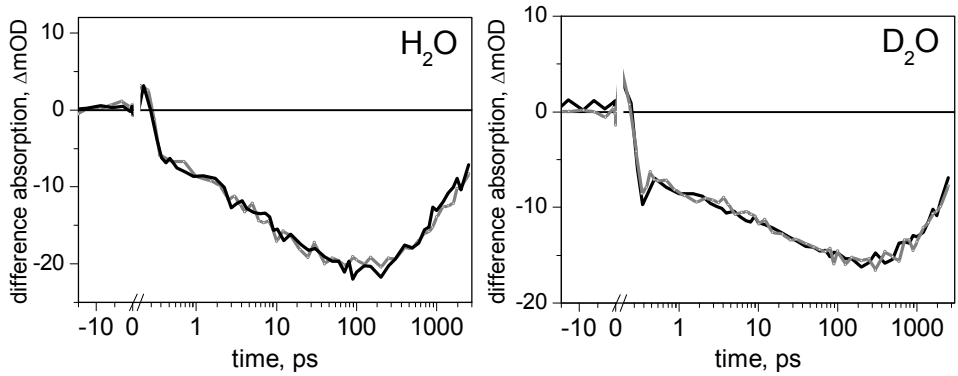

Figure 3.12. Traces of transient absorptions in POR:Pchlide:NADPH recorded at 670 nm upon 475 nm laser excitation in H_2O Tris/Triton buffer **(left panel)** and in D_2O Tris/Triton buffer **(right panel).** The signals are normalized on the amount of accumulated Chlide, i.e. on the amplitude of the signal at 0 ps delay. Grey lines are the signal recorded at 670 nm on fresh and homogeneously CW pre-illuminated POR samples for 30 seconds, black lines are the signals at 670 nm recorded after the sample was kept in the dark for about 24 hours. The experimental procedure corresponds to protocol 4 in figure 3.9.

The latter was confirmed in an additional experiment that was carried out in the same manner, but in which less scans were recorded and the dark period was longer. The sample was first CW illuminated and only one sample scan was taken and after that it was kept in the dark for about 24 hours. The next sample scan was taken on the next day and the kinetics were compared. The experimental procedure is visualized by protocol 4 in figure 3.9. The corresponding traces of TA , shown in figure 3.12, indeed demonstrate that there is

no significant change in kinetics between traces recorded immediately after CW illumination and after staying for 24 hours in the dark. The measurement was repeated on 3 identical samples prepared in H_2O Tris/Triton buffer, and 3 samples prepared in D_2O Tris/Triton buffer. Therefore, this result and its reproducibility confirm clearly that the activation of the enzyme complex by light is persistent for at least 24 hours.

3.3.5. Enzymatic activity in second turnover

To determine whether the enzyme retains its activity after turnover and release of the Chlide product, experiments were performed on CW illuminated samples which were mixed with fresh Pchlide afterwards. If we assume that after turnover and upon rebinding of a substrate the active conformation is lost, then we would expect a decrease of the active fraction of enzymes and increase of inactive fraction in this experiment.

We used the following experimental procedure, which can be schematically represented by protocol 5 in figure 3.9. In figure 3.13.A the visible absorption spectrum 1 of a sample which has never seen light (black line) and contains equal initial concentrations of enzymes and Pchlide, is shown. This sample was illuminated with CW light for 5 minutes, leading to the conversion of Pchlide into Chlide (spectrum 2, red line). As the extinction coefficient of the product is 3 times higher than of the substrate[7, 59], we can calculate from these two absorption spectra that the CW illumination resulted in conversion of about 30% of Pchlide into Chlide. Therefore, the same amount of enzymes, have gone through one turnover and have seen two photons.

After that the sample was remixed with fresh Pchlide and NADPH and the visible absorption spectrum 3 was recorded (blue line, figure 3.13.A). The injected fraction of Pchlide made up about 80% of the total absorption at 630-640 nm. The red shoulder in the absorption at 640 nm indicates that injected Pchlide did bind to enzymes that had been activated by the CW light.

In order to test whether the activity of enzyme is retained, this sample with fresh Pchlide and NADPH was placed into the CaF_2 cell with 200 μm optical path length and 25 sample scans were acquired (indicated as N scans in protocol 5, figure 3.9). After the measurements the absorption spectrum 4 was collected. In spectrum 4 the amount of Pchlide in the sample decreased, and the amount of Chlide increased correspondingly, with a factor of 2.8 relative to the amount of Chlide in spectrum 3 present before laser illumination (compare blue and green lines in figure 3.13.A).

We fitted the recorded TA data to model 1, where all fractions are free parameters, and introduced an additional initial concentration of Chlide (C_0), because of the Chlide produced by the CW pre-illumination (in absorption spectrum 3). The obtained fractions are

shown in figure 3.13.B where they are compared to the simulation of the photon flux-dependent conversion of Inactive→Active→Chlide, which would be observed in a sample that has never seen light prior to the experiment. There is an obvious difference between fitted and simulated fractions of active enzymes (red lines, figure 3.13.B), whereas a very good overlap between fitted and simulated inactive and accumulated Chlide fractions is observed (black and green lines, figure 3.13.B) if the fractions are shifted 20 pulses on the photon flux axis. The latter was done arbitrarily to get a good agreement with the simulated curves, because it was not possible to simply recalculate the amount of light received by the sample upon CW illumination into the equivalent number of scans.

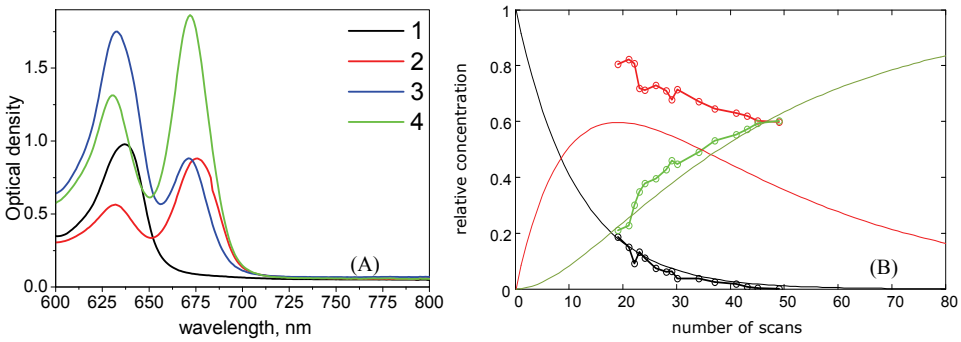

Figure 3.13. (A) The steady-state absorption spectra of POR:Pchlide:NADPH samples with changing illumination history: 1 (black) – a spectrum recorded in the dark with 1 mm optical path. The peak band at 639 nm corresponds to Pchlide bound to the enzyme. 2 (red) – a spectrum recorded after illumination with a CW 40W tungsten lamp for 5 minutes. 3 (blue) – a spectrum recorded after addition of fresh Pchlide and NADPH. 4 (green) – a spectrum recorded after 25 laser scans. **(B)** Fractions of inactive (black dotted line), active (red dotted line) enzymes and Chlide (green dotted line), resulted from the target analysis with fractional model 1 of TA data of 25 laser scans starting at n=20. Simulated concentrations of inactive complexes (black solid line), active (red solid line), and accumulated Chlide (green solid line) derived from model 2 with an excitation rate of 8% and quantum yield of Chlide formation of 30%.

The fact that the amount of active enzymes is higher in the experiment where additional CW illumination was added can be explained only if one assumes that enzymes which have gone through one turnover and then were reloaded with fresh substrate, remained active and therefore, their contribution increased the total concentration of active enzymes. Indeed, in figure 3.13.B the offset in Chlide concentration is 20% relative to the standard experiment, and the same amount is added to the fraction of active enzymes. The

minor fraction of inactive enzymes in the described experiment is due to an incomplete initial conversion upon CW illumination. There is a good agreement in the estimation of the amount of Chlide produced in 25 laser scans, with the amount expected from the steady-state spectra. Comparing the integral absorption of Pchlide band (from 600 to 650 nm) before (blue spectrum in figure 3.13.A) and after 25 scans (green spectrum) we obtain a decrease in absorption of 27%. From the comparison of integral absorptions of Chlide band (from 650 to 720 nm) we obtain an increase in absorption of 52%. Correcting the last number for the 3-fold increase of chlorine extinction coefficient for Chlide[7, 59], the amount of product, accumulated in 25 scans is increased by 17%, very close to the estimations in the target analysis. Hence, we conclude that our model describes the experimental data very well, and that after one turnover, the enzyme remains in the active state capable of photoconverting the next Pchlide to Chlide.

3.3.6. Kinetic isotope effect measurements

We carried out the experiments described in section 3.3.4 (protocol 4 in figure 3.9) in H_2O and in D_2O Tris/Triton buffers in order to see whether a kinetic isotope effect upon H/D exchange was present. The experiments with deuterated and protonated cofactors, i.e. NADPD and NADPH, were done according to protocol 1 in figure 3.9. An accurate conclusion about a change in the rate of the reaction can be made only if the measurements are performed under identical conditions where the same excitation power and optical alignment are used. Therefore, we analyzed the kinetics of Chlide formation for 6 datasets (3 in H_2O and 3 in D_2O) recorded on the same day, under identical experimental conditions, using the global fitting algorithm, and using target fractional model 1. Amplitude model 2 was developed to fit series of gradually changing datasets and therefore, can not fit single scan dataset where there is no sequential evolution of the inactive, active and product fractions.

The traces of transient absorptions recorded at 670 nm in H_2O and in D_2O, depicted in figure 3.14, show an evident difference in the kinetics. The traces were normalized on the amplitudes of the negative signals at t = 0 ps time delays. The kinetics can be attributed to the gain of SE due to formation of I675* and recovery of directly excited Chlide to the GS and to. The amount of accumulated Chlide, varying between 18–40% is indicated in figure 3.15.B. Comparison of all traces in H_2O and D_2O reveals faster appearance of the negative signal of I675* SE in H_2O than in D_2O and the corresponding time constants obtained in global fitting are evidently longer in the case of D_2O compared to H_2O (table 3.2). Note that the full width half maximum (FWHM) of the IRF estimated in global analysis was on average 110 fs with standard deviation of 1.2 fs in all experiments.

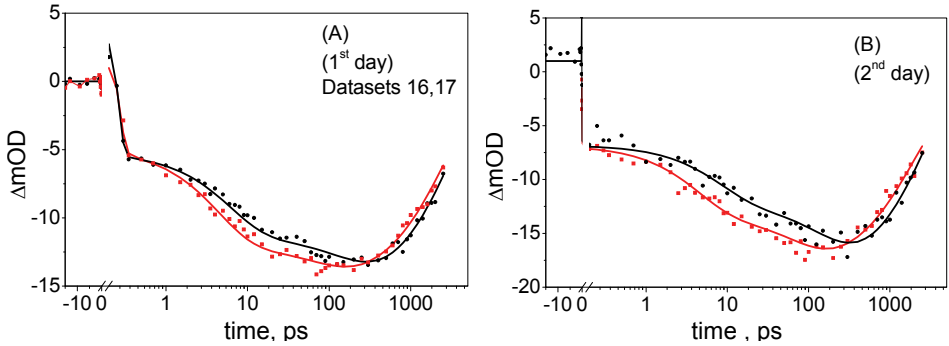

Figure 3.14. Data and global fit of the TA signals recorded in protiated and deuterated enzymes in combination with NADPH. H_2O Tris/Triton POR:Pchlide:NADPH sample (red lines and dots), and D_2O Tris/Triton POR:Pchlide:NADPH sample (black lines and dots). **(A)** Measurement performed after CW illumination, **(B)** Measurement performed on the same samples after 24 hours in the dark (according to protocol 4 in figure 3.9).

Table 3.2. The lifetimes in picoseconds of exponential components found in the sequential global analysis for two solvents.

1st day				2nd day			
sample	t1	t2	t3	sample	t1	t2	t3
H_2O 1	2.1	59	2580	-	-	-	-
H_2O 2	4.3	87	2460	H_2O 2	4.3	76	1877
H_2O 3	6.3	129	2510	-	-	-	-
statistics	mean 4.2 st.dev. 2.1	mean 91.6 st.dev. 35.3	mean 2516 st.dev. 60.2	-	-	-	-
D_2O 1	3.1	99	3040	D_2O 1	8.1	166	3000
D_2O 2	6.1	172	3140	D_2O 2	5.2	123	3200
D_2O 3	3.1	98	3290	D_2O 3	6.12	125	2840
statistics	mean 4.1 st.dev. 1.7	mean 123.3 st.dev. 42.1	mean 3150 st.dev. 125	statistics	mean 6.4 st.dev. 1.5	mean 140 st.dev. 24.3	mean 3010 st.dev. 180

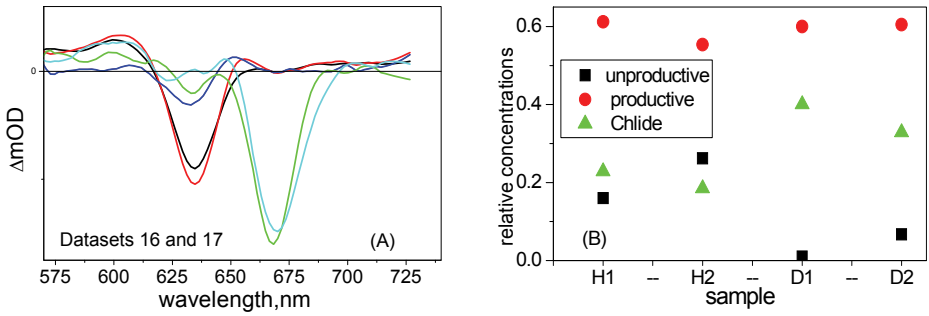

Figure 3.15. (A) SADS obtained in the simultaneous target analysis with free fractional model 1 of protiated and deuterated enzyme in combination with NADPH. **(B)** Relative concentrations obtained in free fractional model 1 for two solvents. The samples H1, H2 are indicated as dataset 16 in table 3.1, samples D1, D2 are indicated as dataset 17 in table 3.1.

Despite the fact that the global fitting does not resolve spectrally different species that are present in the sample, it validates the presence of a KIE upon H_2O/D_2O exchange. The average of ratios $t2_D/t2_H$, $t3_D/t3_H$ is 1.48 which indicates a KIE and thus, the involvement of protons in the reaction, whereas $t1_D/t1_H$ is 0.97 indicating no change in reaction rate.

In the target analysis (figure 3.15), all datasets were fitted simultaneously to the kinetic scheme in figure 3.4, in which the rates in the unproductive branch were restricted to be identical in both solvents and independent of H/D exchange (i.e. θ1, θ2, θ3, θ4), whereas the rates of product formation θ5, θ6 and θ7 were allowed to vary for the different solvents. All fractions were free parameters in the model. It was assumed that corresponding species in both solvents are undistinguishable, i.e. all corresponding SADS in H_2O and D_2O were set identical to each other. The time constants found in this case were 6.3 vs 12.2 ps for Pchlide*I→I675*, and 51 vs 169 ps for Pchlide*II→I675*, which results in KIE ratios of 2 and 3 respectively. In order to facilitate the fit to converge closer to the average values, found in series of experiments (see table 3.1) we tested a model with the Pchlide*II→I675* rate in H_2O fixed at 150 ps. In this case, the KIE ratio for Pchlide*II→I675* was reduced to 1.38-1.62, depending slightly on the relative fractions assumed for each dataset, and the ratio Pchlide*I→I675* was about 2. A similar good quality of fit was obtained in all tested models. SADS are presented in figure 3.15.A. The relative fractions for each experiment were estimated in the target analysis as well (figure 3.15.B). Fractions of productive enzymes in all cases were estimated to be rather high and varied between 48 to 63%, also a reasonable estimation of the amount of accumulated Chlide between 16 and 38% was found in all tested models, the fraction of unproductive enzymes varied between 1 and 27%. We checked that the variation in the fractions does not affect the rates of I675* production and therefore, we exclude that the observed isotope effect on the rate of Pchlide*I (θ5) and Pchlide*II to I675* (θ6) is due to an error in determining the active and inactive fractions. The variation in these fractions can be explained by the slightly different time of initial CW illumination and variations in the initial concentrations, since several stock sample preparations were used in the experiment. As appears from the simulations (see for example figure 3.8.A, B) the highest relative amount of productive enzymes, roughly between 50-60%, can correspond to a very wide range in concentration of unproductive enzymes and Chlide, depending on the amount of previous illumination. Therefore, the simultaneous fit of several single datasets with different conditions is a difficult task, which results in slightly different rates of I675* formation from the typical ones found in the analysis of series of sample scans.

It should be iterated that EADS (evolution-associated difference spectra) derived from the global analysis do not represent spectra of real distinct species and are interpreted only as a weighted sum of SADS (species-associated difference spectra). The rates in the global fit cover not only the product formation, but also the spectral dynamics of both inactive and active complexes, where we assume no dependence on H/D substitution. Therefore, a real physically meaningful KIE can be obtained only in the target analysis. However, the global analysis is a simpler way to demonstrate that the difference in the kinetics upon H/D substitution is not a consequence of difference in the IRF and relative time shift in two measurements, and therefore is not an artifact.

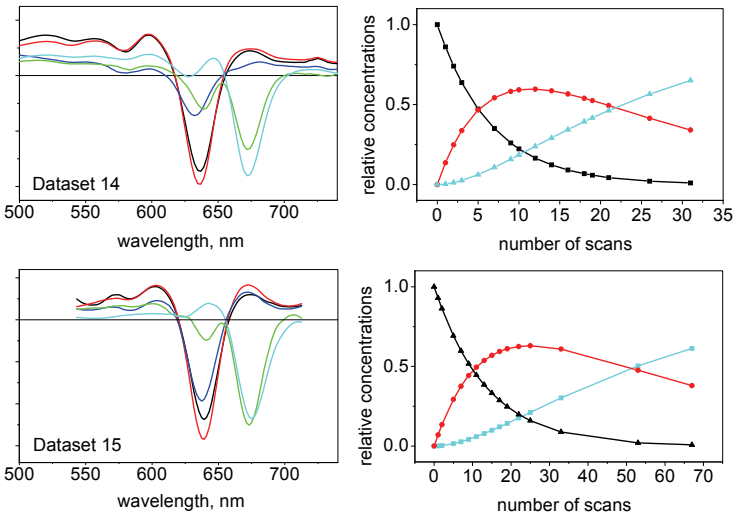

Figure 3.16. SADS and fractions obtained in analytical model 2 for the protiated enzyme in combination with NADPD, i.e. in H_2O Tris/Triton POR:Pchlide:NADPD sample (datasets 14, 15). The corresponding time constants are shown in table 3.1.

In the POR reaction mechanism there are two proton donors, which can be replaced by a heavier isotope deuterium (see scheme in section 3.1). In the experiment with protiated and deuterated enzyme we obtained a difference in the rates of the I675* formation, which suggests that proton transfer is involved in the reaction. Similar experiments have been done on samples in which the second proton donor was replaced with deuterium, namely we used the protiated enzymes in combination with NADPD compared to protiated enzymes with NADPH. The analysis of the data did not reveal any significant difference

between NADPH and NADPD containing samples. The results of these measurements are shown in figure 3.16, and as no evident KIE was found, all SADS and fractions profiles are in line with the data described earlier. The absence of KIE in the rate of the I675* formation when NADPD is used implies that only proton transfer from the tyrosin takes part in the I675* formation. Thus we have tested both possibilities to resolve the sequence of events occurring on the picosecond timescale in the active site of POR. We return to this point later in Discussion.

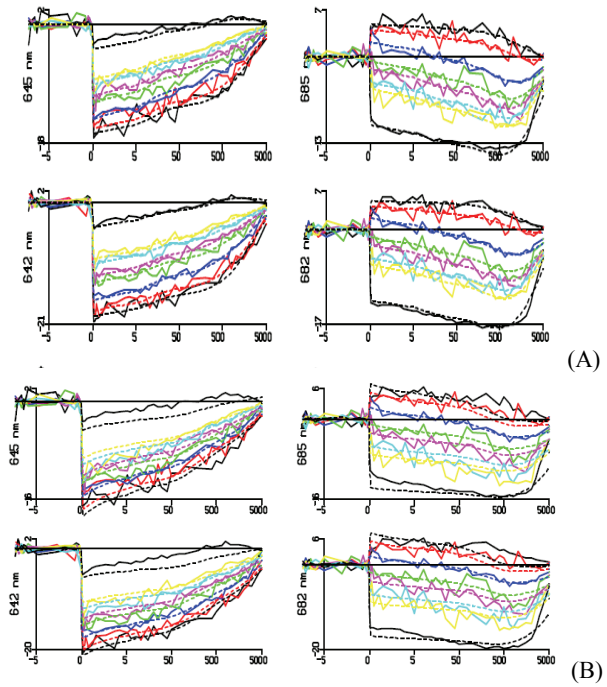

Figure 3.17. Time traces recorded at 642, 645, 682 and 685 nm. Scans 1-2 (black lines close to red), 3-5 (red), 6-18 (blue), 19-25 (green), 26-35 (magenta), 36-45 (cyan), 46-55 (yellow), 55+ CW illumination (black close to yellow). Scans 36-45 were measured in reversed-time direction to exclude that the illumination effect is caused by changing sample conditions during a scan. The time traces are the average of traces recorded on three freshly prepared samples. The dotted lines are the fit resulting from the model described in figure 3.4 with inactive branch included in the model (**A**), and with inactive branch constrained to 0 (**B**).

3.3.7. Validity of the model

To illustrate that the complex kinetic model we have presented here and earlier in chapter 2 and Sytina[52] *et al*, is needed to obtain a good fit of the data, we tested the hypothesis that all enzymes are active in all scans. The concentrations of inactive compartments were constrained to zero, and data was fitted only to the active branch of the kinetic scheme. The resulting fits of transient traces (corresponding to dataset 4) are shown in figure 3.17, where a significant misfit of the data is clearly seen, as compared to the quite acceptable fit obtained with the "full" model, where photon flux-dependent inactive and active fractions are allowed. We note that despite the complexity of the kinetic model, realistic and physically meaningful spectra and rates are obtained from the target analysis. The quality of the fit is judged by inspection of the singular values from the matrix of residuals. The residuals should be structureless, an example of which is shown in chapter 2, figure S3.

3.3.8. Aggregated state of photoactive complex

Besides photoconversion of Pchlide into the I675* intermediate, other processes of emission decay may significantly contribute to the initial dynamics of aggregated Pchlide on an ultrafast timescale. In figure 3.18 a selection of data measured in mesophilic and thermophilic enzymes is shown, which clearly demonstrate unusually broad signals peaking at 660 nm with lifetimes shorter than 1 ps (black). A significant portion of the 660 nm SE-signal decays within 1 ps, thus forming the next 10 nm blue shifted broad spectra peaking approximately at 650-652 nm (red). After about 7-12 ps the third spectrum is formed (blue), which has distinct negative bands at 644 nm and 675-677 nm, likely originating from GS bleach of the substrate and SE of I675*. The I675* band appears mainly in the second and third rounds of the experiment (middle and bottom graphs in figure 3.18). The final state with the blue shifted and reduced in amplitude bleach at 640 nm, and with the 675-677 nm bands slightly increased in amplitude, has a fairly long lifetime, on the order of a few nanoseconds.

Despite the fact that, in this experiment the POR/TPOR samples have some fraction of aggregated pigments, either bound or unbound to the enzyme, they are still highly active, and the formation of the I675* intermediate is similar to that observed in the absence of aggregation. Again the thermophilic enzyme produces less I675* intermediate in the first and second rounds (upper and middle graphs in figure 3.18) when compared to mesophilic enzyme, similar to the experiments discussed in section 3.3.2.

The appearance of red emission in Pchlide and the phenomenon of its fast decay is described in more detail in chapter 6 and 7. Briefly, the appearance of broad short-lived red

states in Pchlide is indicative of Pchlide aggregation, which depends on the preparation and sample conditions. Later in the thesis we show that these states can be formed in neat water solutions without or at very low concentrations of detergent, also in mixtures of organic solvents with water. In POR sample preparations we can eliminate pigment aggregation by adding 1% Triton X100 or Genapol detergent content, as seen from the absence of broadening, red shift and fast quenching of SE (in all POR/TPOR figures except figure 3.18). The lifetimes of the first and second EADS in figure 3.18 found in the enzyme preparation, are very similar to the lifetimes of the two initial EADS for Pchlide in neat water. Therefore, we can assume that the first two EADS in figure 3.18 consist of GS bleach and SE originating from a short-lived red state, which is excited simultaneously with the substrate bound to the protein. It is likely that the sequential loss of SE of this short-lived red state occurs in parallel and obscures spectral dynamics in the blue states, which finally appear.

Also, we note that there are several known spectral forms of Pchlide *in vivo*, minor 633, 643, 669, 680, 690, 698, 728 nm forms, but the dominating and photoactive species is known to be the 655 nm form[4]. The broad and short-lived 650-660 nm states observed in our data are spectrally very similar to the 655 nm *in vivo* form. The appearance of the 655 nm form *in vivo* was mainly assigned to the formation of protein aggregates, either dimers, or tetramers[4].

Figure 3.18. next page. EADS resulting from the global analysis of transient absorptions of aggregated mesophilic **(left column)** and thermophilic **(right column)** POR:Pchlide:NADPH solution with reduced amount of Triton in solvent. Top panels correspond to scans 1-3, middle are scans 4-7, bottom are scans 13-17.

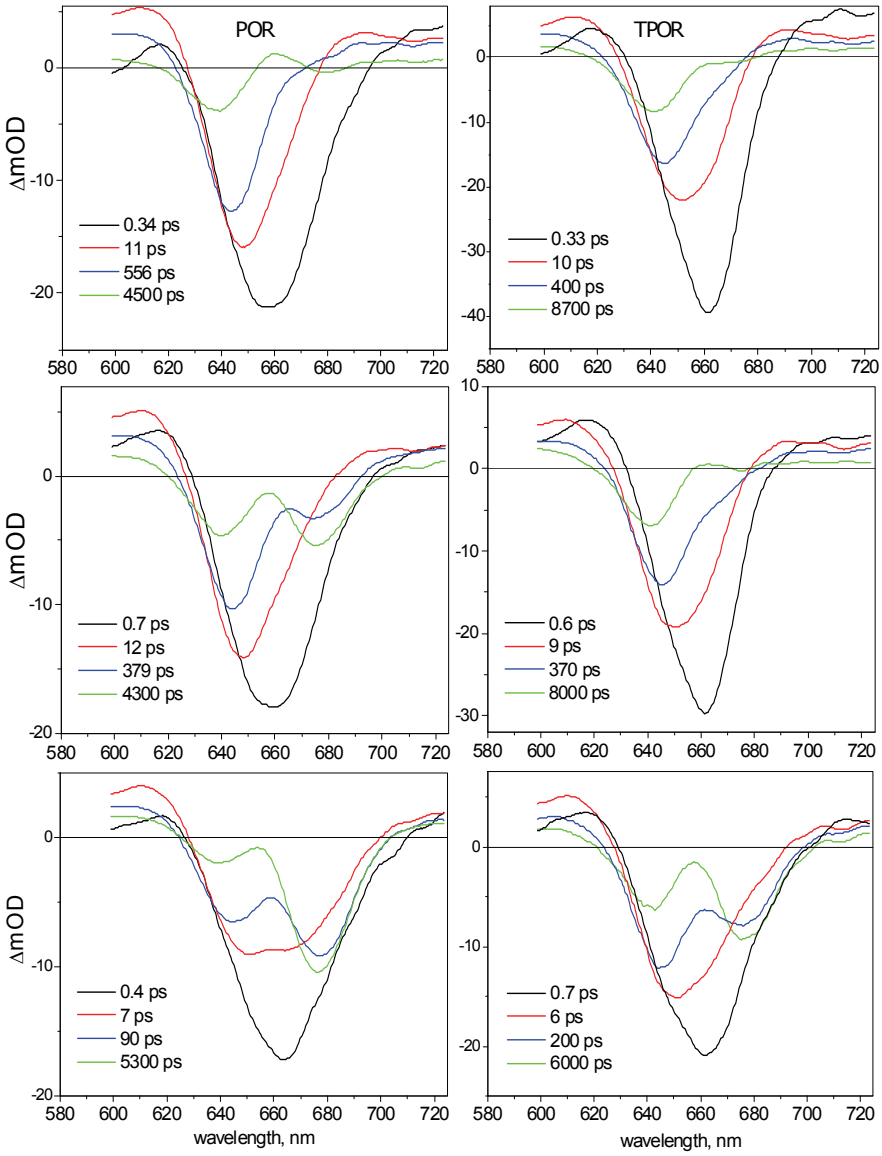
POR
TPOR
ΔmOD
0.34 ps
11 ps
556 ps
4500 ps
0.33 ps
10 ps
400 ps
8700 ps
0.7 ps
12 ps
379 ps
4300 ps
0.6 ps
9 ps
370 ps
8000 ps
0.4 ps
7 ps
90 ps
5300 ps
0.7 ps
6 ps
200 ps
6000 ps
wavelength, nm
wavelength, nm

3.4. Discussion

3.4.1. POR kinetic model

In this chapter the experimental and analytical methods for studying ultrafast catalytic processes in the unique light-driven chlorophyll biosynthetic enzyme POR have been described. From all the collected data we can generate the following generic picture of the ultrafast photoreactions in the POR:Pchlide:NADPH complex. In order to adequately fit the TA dynamics the total population of POR complexes in the sample needs to be divided into inactive and active fractions. The relative concentrations of both are functions of the illumination history of the sample. The spectral evolution of the inactive fraction, which has never been previously excited with a laser pulse, can be described by the inclusion of three excited states, Pchlide*I, II and III, decaying sequentially with rates θ1, θ2 and θ3 respectively. In parallel to this process, the active fraction, which has been excited previously with a laser pulse, can form intermediate product I675* from the states Pchlide* I and II with rates θ5, and θ6. Both enzyme fractions are spectrally undistinguishable and therefore, in the analysis are represented by three spectra, indicated in black, red and blue (see for example figure 3.10). We can also reasonably estimate the spectra of the first catalytic intermediate I675* and of the accumulated final product, Chlide*. In one analytical model, the fractions of active and inactive enzymes in each sample scan are free parameters, and in the second model they are restricted to a sequential mechanism, involving transformation of initially inactive into active enzymes with increasing illumination. The kinetics of the activation mechanism was summarized in figure 3.4 in the Material and Methods section.

3.4.2. Species-associated difference spectra

The datasets obtained in the different series of experiments, using freshly prepared dark samples, in separate experimental sessions, have been analyzed using both models. The large number of experiments allowed us to estimate the variation in the fitted spectra, as well as in the parameters of the fit, i.e. rate constants, fractions of active and inactive enzymes, and quantum yield of product formation. The estimated parameters are collated in table 3.1 for 17 datasets; the corresponding spectra and fractions are shown in figures 3.8, 3.10, 3.15 and 3.16.

First, in figure 3.10 we compare the merits of model 1 and model 2. Due to the reduced number of free parameters in analytical model 2, we could better estimate the gradual change in relative concentrations of inactive and active complexes upon increasing

illumination, and better disentangle the I675* and Chlide spectra. In the free fractional model 1, the amount of active complexes (red lines) tends to saturate with increasing scan number in later scans, and in earlier scans the decay speed of unproductive fractions (black lines) is higher than the formation of productive fractions (red lines) and thus, the product accumulation in fact outruns the productive fraction. The mentioned discrepancy is overcome in the amplitude model 2, where gradual sequential dynamics are imposed, which are, in our opinion, more realistic: unproductive(black)→productive(red)→product (cyan), upon the absorption of a photon. Also, it allows us to minimize the effect of heterogeneity across the sample and resulting scatter in the fractions. Despite the abovementioned problems, model 1 certainly has the advantage in its capability to fit single scan datasets (and was used to fit the KIE results in section 3.3.6), and moreover, it allows estimating discontinuities in illumination. Therefore, we used it to fit the activation-lifetime experiments in section 3.3.4.

In the series of experiments we observe variations in the spectral shapes and ratio of accumulated Chlide and newly formed I675* (green and cyan spectra in figure 3.10), as well as the speed of product formation as a function of scan number for different sample preparations. The different ratios of accumulated Chlide bands and I675* bands in different sample preparations can be caused by the excitation of Pchlide and Chlide in different proportions, at the particular excitation wavelength used, which may have varied a few nm (from 475 to 480 nm) between experiments. The amplitude of the SE signal at 675 nm is about two times larger than that of the Pchlide bleach in the I675* spectrum. This most likely represents an increase in the chlorin extinction coefficient, going from Pchlide to the I675* state.

There is a difference in intrinsic Pchlide* dynamics (black to red to blue evolutions) when 475 nm or 640 nm excitation is used. In the case of blue excitation, the initial black spectrum evolves into a more intense red spectrum (figure 3.10, dataset 5, 6, 7), whereas a gradual decrease of red compared to black is observed upon direct excitation of the Q_Y at 640 nm (figure 3.10, dataset 8, 9, 10). The effect of emission gain upon blue excitation is observed also in neat Pchlide solutions and will be described later in chapter 5 in more detail, but mainly it is related to the S2 to S1 relaxation process and vibrational cooling.

Similar to Pchlide in solution, the final Pchlide* spectrum has a more blue zero-crossing and is, to a varying extent, even blue shifted relative to the earlier Pchlide*I, II spectra. In cases where this spectrum is blue shifted and has reduced excited state absorption, there is a trend that formation of this state with θ2, is slow, see for example datasets 3 and 4. It is possible that here we should have allowed for the formation of a triplet state in the model, and that this omission to a varying degree influences the spectrum and rate constants associated with Pchlide*III. In chapter 5 it will be shown that the blue

shift in Pchlide* dynamics is because of the transition to a triplet state, which leads to loss of the relatively intense Pchlide excited state absorption and of the red stimulated emission.

3.4.3. Kinetic parameters of Thermo- and Mesophilic POR

We established that the amount of product in the POR photoreaction depends on the illumination history of the sample. The earliest catalytic event in the POR reaction involves a transformation of the native inactive enzyme configuration into the active state upon absorption of a first photon. Upon absorption of a second photon the catalytic intermediate referred to as I675* is formed, which eventually leads to Chlide formation:

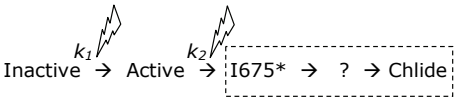

In this scheme k_1 denotes the excitation rate, and $k_2 = k_1 \cdot QY_{Chlide}$, is the excitation rate with which active Pchlide-enzyme complexes are finally converted into Chlide. The excitation rate k_1 can be estimated using model 2 and on average, it was found to be 10% of the rate of excitation in the different experiments. The variation between excitation densities among datasets is probably because of minor differences in the wavelength maximum of the excitation pulse in each experiment. Since the excitation was at the base of the Soret band, this can affect the excitation density. Also, the amount of bound and unbound Pchlide in the reaction mix, which is very difficult to take into account in the modeling, may have affected the effective excitation rate. However, all of our experimental estimates, as described in the Materials and Methods section, return a significantly lower excitation density of only ~5%. It is important to realize that the *excitation rate* for the activation step is in fact a convoluted number, determined by the excitation density per pulse, the number of pulses per scan and the quantum yield of activation. For simplicity, we assumed one time scan to illuminate every spot in the sample once. But, although the asynchronous Lissajous sample scanner (figure 3.2) provides single pulse per spot conditions for the major part of the sample, there are areas at cross points of the Lissajous traces which are doubly excited in one sample scan. We therefore conclude that the excitation density per pulse is 5%, but that one spot is illuminated by effectively 1-2 pulses during one time scan. In some datasets the laser excitation power was deliberately increased in the experiment (datasets 5,7), which resulted in a high estimate of the excitation rate.

Experiments in which measurements on thermophilic and mesophilic POR were performed 'back to back' allow a direct comparison of the estimated excitation densities. In both cases, a two–fold lower effective excitation density is obtained for thermophilic POR, which implies a reduced quantum yield of the activation process. In other words, to our best

estimate, in mesophilic POR the absorption of a first photon results in 100% activation of the enzyme, whereas in thermophilic POR the absorption of a first photon only has a 50% chance of activating the enzyme. Possibly, in the thermophilic enzyme, at RT, the overall rigidity of the protein backbone may reduce the quantum yield of activation and thereby, lead to a slower accumulation of product. Notably, no difference in the rate of I675* formation between thermophilic and mesophilic POR is observed. Basically, these results indirectly confirm the conclusion made earlier in chapter 2 about conformational changes being involved in the activation process and supports the idea of conformational rigidity in enzymes at lower temperatures. In addition, it should be noted that previous work by Heyes and Hunter also observed minor differences in the catalytic cycles of mesophilic and thermophilic enzymes. According to their study, there are two additional catalytic steps in the cycle of the thermophilic enzyme related to $NADP^+$ release and NADPH re-binding events identified by trapping the reaction intermediates at low temperatures[38].

The trigger for the activation process may be the changed electronic distribution in the excited state, or the triplet state, which has a microsecond lifetime. This may possibly involve some specific triplet chemistry, although not with oxygen, since the POR enzyme is functional under anaerobic conditions (D.J. Heyes, unpublished results). Unfortunately, at the moment we cannot provide an estimate for the Pchlide triplet quantum yield in inactive enzymes, since we did not include this state in the model.

From the increase in Chlide concentration as a function of the number of illuminations or laser pulses, we can also estimate the rate k_2. Again, this is a convoluted number, determined by the excitation density per pulse, the number of pulses per scan and the quantum yield of Chlide formation. Relative to k_1, the quantum yield in active enzymes of Chlide formation is on average 0.26±0.06 in mesophilic and thermophilic enzymes for the different datasets, as shown in table 3.1. This estimate is in good agreement with that for the Chlide quantum yield in mesophilic POR of 0.21, based on steady-state measurements[19].

We can also obtain an estimate for the quantum yield of I675* intermediate product formation in activated enzymes, from the following expression:

$$QY_{I675^*} = \frac{\theta_{product}}{\theta_{ex.state}} = \frac{\theta_{product}}{\theta_{product} + \theta_{loss}}$$

where $\theta_{product}$ and θ_{loss} refer to the rates towards the I675* state and to the Pchlide*II (or Pchlide*III) state respectively, thus the formula can be expressed in the following way:

$$QY_{I675^*} = \frac{\theta_5}{\theta_5 + \theta_1} + \frac{\theta_1}{\theta_1 + \theta_5} \cdot \frac{\theta_6}{\theta_6 + \theta_2}$$

which results in 0.68 ±0.11 yield.

3.4.4. Kinetic isotope effect

The results of the target analysis of the 15 datasets summarized in table 3.1, demonstrate that the appearance of I675* intermediate in POR proceeds with average rates of θ1+θ5 = $(3.7 \pm 2.1 \text{ ps})^{-1}$ and θ2+θ6 = $(178 \pm 100 \text{ ps})^{-1}$, with yields of 0.36 for the first step and 0.32 for the second step, giving a total I675* quantum yield of 0.68. The time constants are in accordance with those previously reported of 3 ps and 400 ps by global analysis[20]. The first 3 ps process was previously tentatively assigned to the proton H+ transfer from the tyrosine residue of POR to the C18 position of Pchlide, and hydride H– transfer, from NADPH to the C17 position of Pchlide, was assigned to the 400 ps component. In subsequent measurements on much slower time scale, a KIE effect of 2 upon NADPD/NADPH replacement was resolved for formation of the 696-nm intermediate, and a subsequent solvent KIE effect of 2.2 for the appearance of the 680-nm absorbing intermediate, suggesting that the H-transfer reactions occur in a sequential mechanism on the microsecond timescale[55]. Here, we performed measurements on the isotope substituted complexes to shed more light on the nature of the early intermediates.

The Kinetic isotope effect (KIE) is the phenomenon that a chemical reaction rate may depend on an isotopic substitution, for example a change in the proton transfer rate upon hydrogen to deuterium substitution. Usually, it is denoted as the ratio of the rates KIE = k_D/k_H. Physically, the KIE is related to the difference in masses of the atoms participating in the reaction. Since the energy of the quantum system $E_0 = h \cdot \upsilon(n + \frac{1}{2})$ (taking the simplest case of a harmonic oscillator) is directly proportional to the frequency of the chemical bond, $\upsilon = \frac{1}{2\pi} \cdot \sqrt{\frac{k}{\mu}}$, where $\mu = \frac{m_1 m_2}{m_1 + m_2}$ is reduced mass. Hence, as mass increases then the zero-point energy (ZPE) E_0 decreases, thus making a reaction activation energy barrier higher. Using this approximation a change in a carbon-hydrogen bond to a carbon-deuterium bond of the proton donor should results in a KIE ~1.4 . The KIE can be higher if quantum tunneling is involved [60].

Our data, described in section 3.3.6, clearly demonstrate a difference in the kinetics of I675* formation on the ultrafast timescale between proton and deuterium substituted samples, which is an indication of the involvement of proton transfer into the process. The KIE in the first rate, θ_5, is about 2, and in the second $\theta_6 \approx 1.5$.

Therefore we have now the situation that a NADPH/NADPD kinetic effect is observed only on the microsecond time scale for the formation of the 696-nm intermediate, confirming that the hydride transfer takes place after I675* formation, but solvent KIE's are observed both for the formation of I675* on the picosecond time scale, and for the formation of the 680-nm state on the microsecond time scale. There may be two explanations for a double solvent KIE. The first would be that the I675* state corresponds to a tightly hydrogen-bonded Pchlide state formed after excitation, priming the Pchlide for the actual hydride and proton transfer occurring on the microsecond time scale. However, when Pchlide is bound in the active site of the protein it is likely to have formed a strongly hydrogen-bonded complex already, since binding of Pchlide to the protein causes a 10 nm red shift in the absorption spectrum. Moreover, by fluorescence line narrowing experiments, described in chapter 4, we determined that the keto carbonyl group of Pchlide is downshifted by approximately 50 cm^{-1} when bound to the enzyme, which is clear evidence for a strong hydrogen bonding between Pchlide polar residues and protein residues. While it is possible that I675* corresponds to the formation of additional hydrogen bonds between Pchlide and protein residues, we should also consider the possibility that the KIE of I675* formation is due to the actual proton transfer process, generating Pchlide*-H^+ and Tyr^-, which is then followed by hydride transfer on the microsecond time scale. Why would then a second solvent isotope effect be observed on the microsecond time scale? Possibly, this is due to the reprotonation of the tyrosine radical, which shifts the absorption spectrum of Chlide from 696-nm to 680 nm by a Stark effect. Note, that indeed the 16 nm shift associated with this KIE is significantly smaller than the spectral shift associated with the I675* KIE, of 35 nm (from 640 nm to 675 nm). Further experiments allowing an unambiguous decision between these two scenarios are necessary.

3.5. Conclusions

We have presented the results of carefully designed experimental procedures with well defined illumination conditions together with kinetic modeling, and systematic analysis of many datasets that revealed a number of major properties of POR:Pchlide:NADPH complexes.

1) First, by fitting series of single pulse sequential experiments it was found that the existence of two forms of enzyme complexes are needed to describe the experimental data. The highly non-linear dependency of product accumulation is caused by a two photon activation mechanism, when initially inactive enzyme complexes become active upon absorption of the first photon, whereas the second photon initiates the reaction.

2) The quantum yield of activation is lower by about 50% in thermophilic enzyme as compared to mesophilic enzyme, at RT. This may be due to increased conformational rigidity in the thermophilic enzyme at RT.

3) We demonstrated by comparing kinetics measured first on the pre-illuminated enzyme and then after keeping the sample in the dark for 24 hours that the active state of enzyme has a very long lifetime, and that the active state survives the first turnover.

4) By comparing TA dynamics in the samples prepared on the basis of H_2O and D_2O we demonstrated the presence of a kinetic isotope effect on an ultrafast timescale, associated with the formation of I675*. By kinetic modeling we found that the ratio between the rates of product formation is close to 2 for the 3-ps rate formation and ~1.5 for the 150-ps rate formation.

5) We demonstrated that there is a spectroscopic resemblance between several mesophilic and thermophilic POR TA datasets under low detergent concentrations and the previously known photoactive 655 nm Pchlide form *in vivo*. We suggested that the red shift, broadening and ultrafast loss of SE signal is determined by the aggregation of Pchlide, whereas the POR complexes are not likely to form aggregates.

In conclusion, the combination of a convenient model system such as the light-dependent POR enzyme with carefully designed kinetic experiments allows the real time observation of catalytic reactions. The main result of the current study demonstrates explicitly the importance of conformational changes for initiation of a catalytic turnover. It has been shown recently that conformational changes in the POR enzyme are involved in the sequence of product release steps as well[61]. The fact that the activated state is not lost in the second turnover and is long-lived suggests that perhaps there is a minor adjustment of protein residues in the binding pocket of the active site which is not influenced by major rearrangements upon binding and release events. Since the appearance of the active fraction occurs mainly in the second sample scan and the time interval between scans is about one minute we may assume that the conformational change takes place within this period of time. Also, from FTIR measurements[52] we know that the conformational change in POR occurs on a timescale longer than the ns laser pulse at least. The enzyme conformational change may be triggered by changed electrostatic conditions in the active site upon electronic excitation of Pchlide, or by the triplet state of Pchlide.

Our study has led to a better identification of the reaction path at room temperature and the identification of the early intermediate state(s) involved. Further experiments are needed to determine which structural changes lie at the origin of the activation process. Certainly, the isotope labeling of important protein residues will allow us to discover the role of specific amino acids in the enzyme active site. Also, the resolution of the structure

of POR, either by X-ray diffraction, or by NMR techniques will undoubtedly be important in this process.